JOURNAL OF GEOPHYSICAL RESEARCH, VOL. 90, NO. D6, PAGES 10,563–10,585, OCTOBER 20, 1985

A Simple Scheme for Generating Two Layers of Radiatively Constrained Effective Clouds in GCM's

CHARLES T. GORDON, WILLIAM F. STERN, RUSSELL D. HOVANEC[1]

Geophysical Fluid Dynamics Laboratory, Princeton University, New Jersey

GCM-dependent, radiatively constrained cloud amount fields could be preferrable to currently available observed fields for calculating radiative fluxes in GCM's used in long-range weather forecast studies. Motivated by this premise, we formulate an economical effective cloud algorithm for GCM's called "SATCLD," which utilizes compact, readily accessible analyses of observed satellite-derived radiative flux data. We then examine the plausibility of preliminary effective cloud fields. Analysis of SATCLD and other cloud fields and associated radiative fluxes (diagnosed by our GCM's cloud radiation model from observed atmospheric temperature and water vapor data) also provides some insight into biases in our GCM's cloud radiation model and surface albedo field. "SATCLD" generates effective low and high cloud amounts at each GCM grid point by minimizing the sum of the squares of the local residual (i.e., model-diagnosed minus observed) shortwave and longwave radiative fluxes. The preliminary SATCLD effective cloud amount fields seem plausible in many respects, based upon comparison with the satellite-derived 3DNEPH and surface-based SFCOBS analyses. In the tropics the SATCLD effective high cloud amount is rather well correlated with 3DNEPH, while systematic differences in low cloud amount are evident in July. Off the west coasts of Central and South America and southern Africa, the SATCLD effective low cloud resembles SFCOBS in July. At mid-latitudes the strongest similarities are between SATCLD versus 3DNEPH high cloud amount in July and SATCLD versus SFCOBS low cloud amount over the oceans. The SATCLD analysis is ill conditioned in the polar night region. Limitations of the present scheme as well as deficiencies in our GCM's cloud-radiation model and surface albedo fields and in the archived satellite data are discussed. Suggestions are made for reducing discrepancies between effective versus real clouds without sacrificing consistency between GCM-diagnosed versus observed radiative fluxes.

1. INTRODUCTION

This paper focuses on an algorithm called SATCLD, which generates fields of radiatively constrained, i.e., "effective," cloud amounts for general circulation models (GCM's) from compact, accessible analyses of satellite-derived radiative flux data. The motivation and rationale for developing it are discussed below.

It is generally acknowledged that clouds affect the horizontal and vertical distributions of atmospheric radiative flux. In turn the latter may influence the atmospheric circulation through radiative-dynamic coupling, as noted by *Stephens and Webster* [1979; 1981], *Ramanathan et al.* [1983], and others. Hence the radiative treatment and specification of clouds in GCM's is of practical concern to modelers engaged in climate sensitivity or long-range weather prediction experiments.

One of our long-term objectives it to assess the impact of specified, quasi-realistic, cloud radiation forcing upon the predicted atmospheric circulation over the range of 1 month to perhaps one season. A relevant concern is how to specify such forcing within the framework of present generation GCM's, including their cloud radiation models. In this regard, cloud amount is a useful class of variables to work with, considering its prominent role in current generation GCM's as well as in currently available cloud data sets. For our purposes the term "cloud amount" will refer collectively to the respective fractions of a GCM grid box containing low, middle, or high cloud amount.

In GCM's, cloud amount fields are either specified or else parameterized in terms of model-predicted thermodynamical and/or dynamical variables. Various empirical schemes for predicting cloud amount in GCM's have recently been developed, e.g., at the European Centre for Medium-Range Weather Forecasts (ECMWF) [*Slingo*, 1984] and elsewhere. Model-predicted relative humidity is typically the primary predictor, while the predicted static stability and/or vertical velocity may be used as well. However, to minimize the radiative effects of systematic errors (e.g., model climatic drift) in the GCM-predicted temperature and water vapor mixing ratio fields and/or deficiencies in cloud prediction schemes themselves, we confine our attention to specified layered cloud amount fields.

Historically, the available data sets have tended to ignore the longitudinal variability of real clouds, even on the planetary scale. A prime example is the zonal mean, seasonal mean climatology based upon *Telegadas and London* [1954] that was specified for nearly two decades in GCM's at the Geophysical Fluid Dynamics Laboratory (GFDL). Just prior to the initiation of the present study, the situation began to change as some zonally asymmetric cloud amount data sets became available. For example, *Meleshko and Wetherald* [1981] produced a monthly mean climatology for July. Also, monthly mean 3DNEPH, SFCOBS, and (following Meleshko and Wetherald) Meleshko data sets have been generated by *Gordon et al.* [1984, hereafter referred to as GHS] for two specific months. Characteristics of the 3DNEPH and SFCOBS data sets are briefly described in section 2.

Another satellite-derived cloud amount data set for 1979 [*Stowe*, 1984] has only recently become available. Meanwhile, the release of the comprehensive cloud data sets being generated by the International Satellite Cloud Climatology Project (ISCCP) has been delayed.

Clearly, when our work was initiated there was a paucity of global, longitudinally varying cloud amount data sets. Moreover, another concern, raised by GHS's analysis of model-

[1]Currently at Kidder, Peabody and Company, Inc., New York.

This paper is not subject to U.S. copyright. Published in 1985 by the American Geophysical Union.

Paper number 5D0541.

diagnosed radiative fluxes, was whether any of the available data sets would yield reasonably realistic cloud radiation forcing fields. By definition, model-diagnosed fluxes are calculated by a GCM's cloud radiation model from observed (as opposed to model-predicted) temperature and water vapor) fields and specified cloud amount and surface albedo fields. Intuitively, a fairly high degree of consistency between model-diagnosed versus observed long-wave, shortwave, and net radiative fluxes should be one of the prerequisites for generating reasonable cloud radiation forcing fields. But judging from the results of GHS for the GFDL GCM and 3DNEPH, SFCOBS, and Meleshko clouds, radiative consistency is by no means assured when currently available observed cloud amount fields are specified in an arbitrarily chosen GCM. The SFCOBS cloud fields were derived from surface-based observations and hence were devoid of any explicit radiative constraints. In contrast, 3DNEPH and Meleshko were constrained by satellite-derived observed long-wave fluxes. Nonetheless, these constraints were weak or implicit and/or were applied only over certain regions.

Important factors that contribute to radiative inconsistency are deficiencies in (1) the observed cloud amount data set itself; (2) the GCM's cloud radiation model, e.g., parameterizations of cloud top height, emissivity, cloud albedo, etc.; (3) the GCM's surface albedo field and radiative treatment of aerosols; and (4) analyses of temperature, water vapor, and/or radiative flux. Thus radiative inconsistency would be likely to occur, even if the field of observed cloud amount were perfect.

Regarding factors 2 and 3, the cloud radiation model, treatment of aerosols, and/or surface albedo parameterizations of many GCM's lag behind the state of the art empirical knowledge. For example the parameterizations of cloud albedo and cloud emissivity in GCM's could be improved and unified through their mutual dependence upon the cloud liquid water and/or ice content [*Stephens and Webster*, 1981]. However, the latter cloud properties would have to be reasonably specified or accurately predicted. Also, most GCM parameterizations of surface albedo could incorporate more of the potentially important parameters discussed by *Wiscombe and Warren* [1980], *Warren and Wiscombe* [1980], *Robinson* [1984], and others. That list includes snow melt, snow age, grain size, impurities, type of exposed vegetation, and (visible versus near-infrared) wavelength dependence of the spectral reflectivities of snow and vegetation.

Turning to conventional meteorological observations, the analysis of water vapor over the tropical oceans and in the southern hemisphere suffers from a paucity of data. Meanwhile, satellite-derived radiative fluxes are adversely affected by infrequent sampling, narrowness of the visible or infrared bands, neglect of anisotropic effects or zenith angle dependence, etc. [*Cess et al.*, 1982]. Also, the satellite observations and the conventional observations are not concurrent. More specifically, the former are asynoptic, being taken at approximately the same local time, whereas the latter are essentially synoptic.

In short, model-diagnosed radiative fluxes calculated by a given GCM will probably be inconsistent with observation for quite some time if "alien" analyses of observed cloud amount are specified. (An "alien" cloud analysis is produced from different cloud radiation and/or surface albedo models, then the GCM's and/or different analyses of radiation, temperature, or water vapor.) Under these circumstances, modelers could adapt the cloud radiation and surface albedo models of their GCM's to be more compatible with those used to produce the cloud analysis and could compare their model-diagnosed radiances against observation.

But in the interim a simpler alternative strategy (the one proposed here) is to generate "effective" clouds specifically for one's own GCM. In practice it is necessary to broaden the traditional definition of "effective" clouds, i.e., ours are constrained to be as consistent as possible (see section 2) with long-wave and shortwave radiative fluxes. By being GCM dependent, the effective cloud amounts should compensate for the net effect of biases in the GCM's cloud radiation model, surface albedo field, etc., as well as in the observed satellite-derived radiative fluxes and other input data. In fact the adjustment of cloud amount to the observed radiative balance may be compared to the dynamical initialization of the wind field to the observed mass field. An initialized wind field departs somewhat from the true observed field because of the imposition of dynamical constraints. Analogously, the constraint of radiative consistency, i.e., of quasi-realistic cloud radiation forcing, may induce cloud amount fields to depart from the true observed fields.

There are potentially two advantages of specifying effective clouds in GCM's. First, they constrain GCM-diagnosed radiative fluxes to be more or less consistent with observation. This could be beneficial, provided that deficiencies in the analyses of the observed satellite data were not the dominant contributing factor to radiative inconsistencies. For example, the impact of quasi-realistic, cloud radiation forcing fields upon long-range forecasts by GCM's could be investigated before definitive cloud climatologies became available. Second, a comparison of effective clouds and corresponding GCM-diagnosed radiative fluxes with observation would afford modelers the opportunity to become more aware of radiation-related biases in their GCM's as well as in analyses of observed satellite data and perhaps motivate them to improve the treatment of radiative transfer, clouds, aerosols, and/or surface albedo in their GCM's. Through an iterative process, effective cloud fields could become more realistic.

Our immediate objectives are to formulate an algorithm called SATCLD, which generates GCM-dependent effective clouds for GCM's, and to present some preliminary results of its application. We emphasize that no attempt is made to construct a definitive cloud climatology. In keeping with the spirit of the SATCLD approach we have employed a typical GCM, i.e., the GFDL spectral extended range prediction model and a convenient, satellite-derived radiative flux data set, despite some potentially rather serious limitations of both. For example, there are not enough degrees of freedom in the archived radiative flux data currently available to capture all of the important properties that characterize real clouds or to independently validate the SATCLD effective clouds.

Schneider [1972] used the concept of effective clouds to discuss the sensitivity of global mean climate to global mean cloudiness. His variables were global mean effective cloud top height and cloud cover fraction of a single layer of clouds. However, for GCM applications the desired effective cloud top height will not necessarily coincide with any of the fixed vertical levels of the GCM in question. The resulting discrepancy could be rather substantial if the spacing between adjacent levels were to exceed 50–75 mbar in the upper troposphere. In contrast, effective cloud amounts for two distinct cloud layers can be finely tuned to attain radiative consistency locally. Therefore we have modified Schneider's approach such that the variables are grid point values of effective low and high cloud amount, while the cloud tops and bases are fixed a

priori. Global analyses of effective low or high cloud amount can be built up from solutions at each GCM grid point.

Another key feature of the SATCLD scheme is that it utilizes compact, readily available data sets of analyzed long- and shortwave radiative fluxes. The tape volume of archived data requiring processing is relatively minimal, by virtue of its 250–500 km, GCM-compatible spatial resolution. This may be quite advantageous, since it would be unfeasible for most modelers to work directly with pixel-scale radiance data. Moreover, the scheme is economical to apply, at least for two (or three) cloud parameters.

2. Calculation of SATCLD Effective Clouds

2.1. *Formulation of the SATCLD Scheme*

The underlying approach might be categorized as an inverse method. The SATCLD algorithm itself is relatively straightforward. The first step is to expand the available observed satellite-derived data, i.e., analyzed values of absorbed shortwave radiative flux S_{obs} and outgoing long-wave flux F_{obs} as second-order Taylor series in the unknown cloud amount variables. More precisely, at each grid point of our GCM,

$$S_{obs} = S_0 + \left(\frac{\partial S}{\partial n_h}\right)_0 \Delta n_h + \left(\frac{\partial S}{\partial n_l}\right)_0 \Delta n_l + \frac{1}{2}\left(\frac{\partial^2 S}{\partial n_h^2}\right)_0 \Delta n_h^2 + \frac{1}{2}\left(\frac{\partial^2 S}{\partial n_l^2}\right)_0 \Delta n_l^2 + \left(\frac{\partial^2 S}{\partial n_h \partial n_l}\right)_0 \Delta n_h \Delta n_l + \varepsilon_S \quad (1)$$

$$F_{obs} = F_0 + \left(\frac{\partial F}{\partial n_h}\right)_0 \Delta n_h + \left(\frac{\partial F}{\partial n_l}\right)_0 \Delta n_l + \frac{1}{2}\left(\frac{\partial^2 F}{\partial n_h^2}\right)_0 \Delta n_h^2 + \frac{1}{2}\left(\frac{\partial^2 F}{\partial n_l^2}\right)_0 \Delta n_l^2 + \left(\frac{\partial^2 F}{\partial n_h \partial n_l}\right)_0 \Delta n_h \Delta n_l + \varepsilon_F \quad (2)$$

In the above equations, n_h and n_l are the effective high and low cloud amounts, respectively. Also, S and F are model-diagnosed short- and long-wave radiative fluxes, i.e., they are computed by the GCM's cloud radiation model from observed meteorological data. The "0" subscript indicates that the model-diagnosed fluxes or derivatives correspond to known reference values of effective high cloud amount n_{h_0} and low cloud amount n_{l_0}. The unknowns Δn_h and Δn_l represent the departures $n_h - n_{h_0}$ and $n_l - n_{l_0}$, while ε_S and ε_F are residuals. To insure that the above system of equations is not underdetermined, only two layers of effective cloud are solved for. This restriction can be justified, perhaps, on the grounds that surface observers report fewer than three cloud layers approximately 95% of the time. By choosing high and low cloud layers, the contrasts in their long-wave emission and (given our cloud radiation model) shortwave reflectivity are enhanced.

In principle, middle clouds and/or other cloud properties could be added to the list of unknowns (see section 6), given more observed radiative parameters besides F_{obs} and S_{obs}. Alternatively, the latter could be used to help validate GCM cloud radiation models, as has been recently proposed by *First ISCCP Regional Experiment (FIRE)* [1983]. But unfortunately, the archived data sets utilized in our study did not contain these additional parameters.

In any case the desired solution at a particular grid point is the pair of effective cloud amounts n_l and n_h that minimizes the sum of the squares of the residuals in the Taylor series expansions for S_{obs} and F_{obs}. Mathematically, the minimization criterion may be expressed as

$$(\varepsilon_F^2 + \varepsilon_S^2)\{\Delta n_h, \Delta n_l\} = \text{minimum} \quad (3)$$

Equation (3) constrains the cloud amounts n_l and n_h to be approximately consistent with the observed net radiative flux R_{obs}, where $R_{obs} = S_{obs} - F_{obs}$. In other words the squared residual net flux $(\varepsilon_S - \varepsilon_F)^2$ will usually be small, even if not rigorously minimized. Moreover, (3) will tend to exclude solutions whose residuals ε_S and ε_F are individually large but fortuitously cancel. This is a desirable characteristic, since the modulation of long-wave and shortwave radiative fluxes by clouds will be strongest in the upper troposphere and near the earth's surface, respectively, as noted by V. E. Ramanathan (personal communication, 1983). Note that the equation "ε_F^2 = minimum" becomes a good approximation to (3) at high latitudes of the winter hemisphere, where S, and hence ε_S, is small.

The physical realizability constraints

$$\left.\begin{matrix} 0 \le n_h \le 1 \end{matrix}\right\} \quad (4a)$$

$$\left.\begin{matrix} 0 \le n_l \le 1 \end{matrix}\right\} \quad (4b)$$

must be invoked occasionally in order to perform the radiation calculations. This is most likely to occur if the cloud radiation model and/or observed input data contain large biases and/or the effective high or low cloud amount is close to 0% or 100%. Note that the consistency of model-diagnosed radiative fluxes with observation is compromised wherever (4*a*) and (4*b*) are explicitly applied. However, the resulting discrepancy may remain small locally where small fluctuations in radiative flux are associated with large fluctuations in effective cloud amounts.

Although (1) and (2) are nonlinear with respect to n_l and n_h, they are readily solved by trial and error, i.e., by varying n_l and n_h independently in increments of 0.01. The computation time for two cloud layers was quite trivial on the Control Data Corporation (CDC) CYBER 205 computer. If the second derivative terms are discarded, (1) and (2) become linear and could be solved for n_l and n_h by Cramer's rule. However, there is no guarantee that the constraints (4*a*) and (4*b*) will be satisfied, nor is there any computational advantage over the trial and error method. In practice the inclusion of the second derivatives yielded, at best, only a slight improvement in the representation of F and virtually none in the representation of S.

The partial derivatives in (1) and (2) provide a measure of the sensitivity of model-diagnosed radiative fluxes to n_l and n_h, holding all other meteorological variables fixed. They are computed a priori as follows. First, monthly mean or instantaneous initial meteorological conditions are input into a global spectral GCM. A series of one time step integrations is performed from the same initial conditions. In this manner the radiative fluxes are diagnosed in terms of the initial, observed values (as opposed to predicted values) of temperature and water vapor. The only parameters that are varied are the low and/or high cloud amounts. In a particular run the same value of cloud amount, i.e., 0.0, 0.25, 0.50, 0.75, or 1.00 is specified at each grid point on the spectral GCM's transform grid. The determination of n_h and n_l was quite insensitive to two choices of reference cloud amounts in (1) and (2). Therefore we chose $n_{h_0} = 0.50$ and $n_{l_0} = 0.50$ in the Taylor series expansions. The partial derivatives, e.g., $(\partial F/\partial n_l)_0$, $(\partial^2 S/\partial n_h^2)_0$, etc., are estimated by centered finite difference approximations from S(0.25), S(0.50), S(0.75), F(0.25), F(0.50), and F(0.75). Monthly

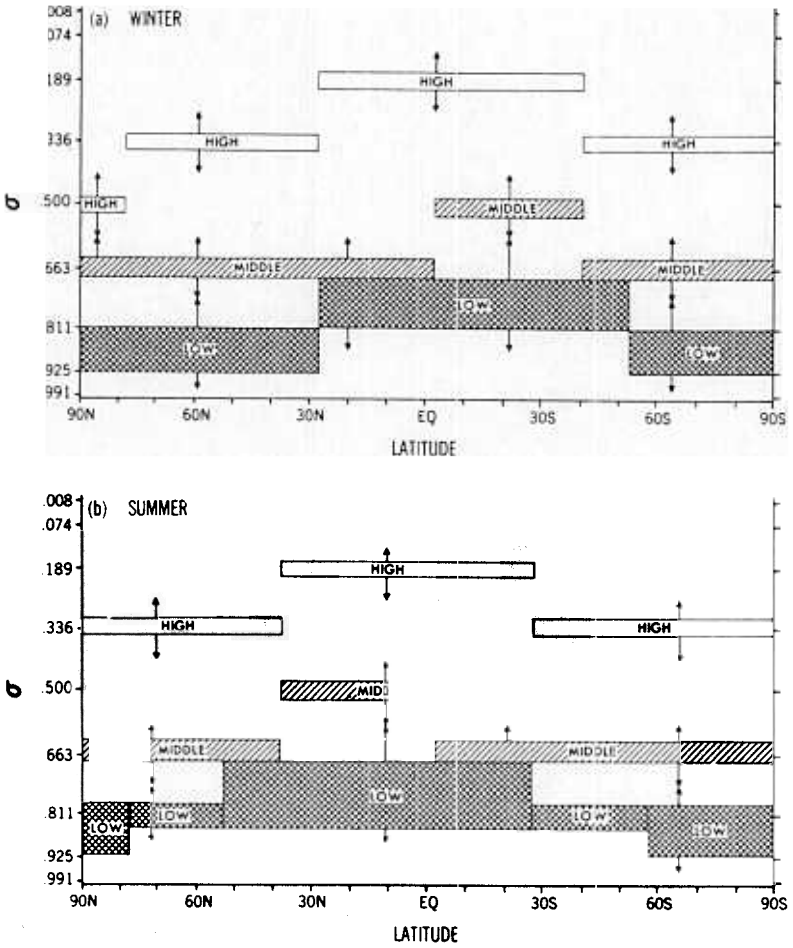

Fig. Schematic diagram of the vertical placement of the clouds in the radiative flux calculations for (*a*) January 1977 and (*b*) July 1979; σ is the vertical coordinate.

mean or daily mean values of S and F are used, respectively, to generate monthly mean or daily analyses of effective cloud amount.

A preliminary check of the computer code and of the validity of the Taylor series expansion over the range of permissible values of n_l and n_h was performed. For this purpose, model-diagnosed fluxes S_M and F_M were calculated for $(n_l, n_h) = (0.0, 0.0)$, $(0.25, 0.0)$, $(0.50, 0.0)$, ..., $(0.0, 0.25)$, $(0.25, 0.25)$, ..., $(1.0, 0.25)$, ..., $(1.0, 1.0)$. Then, n_l and n_h were computed from (1) and (2) with $S_{obs} = S_M$ and $F_{obs} = F_M$. The computed values of n_l and n_h usually agreed with the "true," i.e., originally specified, values to within a few percent. However, larger discrepancies occurred near the poles, where (4*a*) and (4*b*) were frequently applied.

2.2. *The GCM*

A GFDL spectral GCM is used to diagnose radiative fluxes from observed monthly mean or instantaneous meteorological data. This model is rhomboidally truncated at wave number 21, has nine vertical levels, and employs the so-called E4 parameterization of subgrid-scale vertical turbulent mixing, Fels-Schwarzkopf radiation [*Fels and Schwarzkopf*, 1975, 1981], moist convective adjustment, large-scale condensation, orography, hydrologic cycle, etc. The distinctive features of the E4 parameterization are (1) a static stability-dependent Monin-Obukhov formulation in the surface boundary layer; (2) a Richardson-number-dependent, *Mellor and Yamada* [1974] turbulent closure scheme in the planetary boundary layer and free atmosphere; and (3) suppression of dry convective adjustment. The surface temperature is calculated over land and sea ice by solving a surface heat balance equation but is specified over open water. The GCM is commonly referred to as R21L09 E4. An R30L09 E4 version has been described in greater detail by *Gordon and Stern* [1982].

The Fels-Schwarzkopf radiation model is an important component of our GCM. It is considered to be quite respectable for GCM applications. Its features include (1) the *Fels and Schwarzkopf* [1975] simplified exchange method of calculating infrared cooling associated with water vapor; (2) accurate CO_2 transmission coefficients [*Fels and Schwarzkopf*, 1981]; (3) a *Bignell* [1970] water vapor continuum, which varies approximately as the square of the water vapor concentration; (4) the *Lacis and Hansen* [1974] parameterization of absorption by ozone and water vapor; and (5) multiple reflection. One restrictive feature of the Fels-Schwarzkopf radiation model is that model-diagnosed radiances cannot be analyzed for specific narrow spectral bands. Thus it is necessary to verify against observed broadband flux data.

In our GCM the fixed cloud top heights and bases of low, middle, and high clouds are based primarily upon the cloud climatology of Telegadas and London [1954]. They vary with latitude and season as shown schematically in Figure 1. The values are identical for effective and observed clouds, with the caveat that there are no effective middle clouds. The fixed

cloud absorptivities and zenith-angle-dependent cloud albedos are summarized in Table 1. They correspond to the January 1977 standard absorptivities and one of the albedo options of GHS, respectively. All (effective or observed) clouds, including cirrus, are assumed to be blackbody emitters in the infrared, i.e., their emissivity is 1.0.

GHS' model-diagnosed radiative fluxes were sensitive to the emissivity and cloud top height assumed for 3DNEPH high clouds. Similarly, effective high cloud amount should be sensitive to such cloud parameters. Indirect confirmation of this is given in section 3. However, sensitivity experiments of a more controlled nature, which may be interesting in their own right, have not been performed.

The specified field of surface albedo A_s is the same as in GHS, unless otherwise noted. It is based upon the *Posey and Clapp* [1964] analysis over land; the *Payne* [1972] zenith-angle-dependent formulation over the open oceans; and, in January, an AFGWC (Air Force Global Weather Central) weekly mean digitized analysis of snow depth over the northern hemisphere for the first week of January 1977. GCM climatological monthly mean snow cover is specified in the southern hemisphere and in July, in the northern hemisphere. The surface albedo of snow-free sea ice is fixed at 0.50, while $A_s = 0.75$ over land and snow-covered sea ice poleward of 70°. At other latitudes, A_s varies with snow depth as

$$A_s = \min \{A_{s_0} + (0.6 - A_{s_0})(d/10)^{1/2}, 0.6\} \quad (5)$$

where A_{s_0} is the surface albedo for snow-free conditions and d is the snow depth in centimeters. The standard A_s field for July is shown in Figure 4*a*. For January, see Figure 12 of GHS.

2.3. *Observed Radiative Flux Data*

The observed fluxes S_{obs} and F_{obs} were obtained for January 1977 and July 1979 from daily analyses of earth radiation budget data. During those months, the NOAA 5 and TIROS-N satellites were in orbit, respectively. Their daytime equatorial crossings occurred at approximately 0930 hours and 1500 hours local time. The data were archived on a 2.5° × 2.5° resolution latitude-longitude grid by the National Environmental Satellite Data Information Service (NESDIS) according to the procedures described by *Gruber* [1978].

These archived analyses were selected on the basis of their overall convenience, i.e., availability, compactness, user-friendly flux format, and extrahemispheric (global) domain. But as previously mentioned, they may possess some potentially serious limitations. Perhaps most worrisome is the unresolved question of how well the archived values of S_{obs} represent the true diurnal mean values. The limiting factors are the local sampling frequency of the planetary albedo (essentially once per day) along with the assumptions that the albedo is isotropic and not a function of zenith angle. Regarding the latter factor, the archived data utilized in this study is based upon midmorning or midafternoon satellite measurements of reflectivity. Fortunately, these may be more representative of diurnal mean conditions than noontime measurements would have been. Also, as discussed by GHS, the scanning radiometers aboard the NOAA 5 and TIROS-N satellites measured considerably wider visible bands than those aboard some other NOAA satellites. This situation may have favorably affected the conversion of radiances to broadband fluxes for the particular cases investigated here. On the other hand, during the course of our investigation, *Ohring et al.* [1984] confirmed the existence of a bias in the NESDIS long-wave flux data.

TABLE 1. Cloud Albedos and Absorptivities for January 1977 and July 1979 Integrations

	Albedo	Absorptivity
High clouds	0.241 − 0.0677 cos Z	0.005
Middle clouds	0.521 − 0.1548 cos Z	0.020
Low clouds	0.673 − 0.2225 cos Z	0.035

Therefore we recomputed the SATCLD effective clouds and corresponding model-diagnosed radiative fluxes by using correction formulae (see GHS, appendix B) supplied by A. Gruber (personal communication, 1983).

In any case, diurnal mean values of F_{obs} were calculated from the archived daytime and nighttime values. Also, monthly means of S_{obs} and F_{obs} were computed from daily values as needed. Then the archived fluxes were interpolated to our spectral GCM's 3.3° × 5.6° Gaussian latitude-longitude grid.

2.4. *Observed Cloud Amount Data*

For comparison purposes, two analyses of observed cloud amount are utilized later: (1) 3DNEPH is a reconstruction (within the northern hemisphere only) of the voluminous AFGWC 3D-Neph analysis [*Fye*, 1978]. This hybrid analysis uses primarily satellite data plus some timely surface-based observations. The satellite data is obtained from two polar-orbiting military satellites (DMSP) whenever possible. However, during January 1977, NOAA 5 data was used. The 3D-Neph archieve contains cloud amounts at 15 prescribed vertical levels as well as total cloud cover and auxiliary cloud and weather information. The temporal resolution is nominally 3 hours, and the horizontal resolution is approximately 50 km. Each hemisphere is subdivided into 60 regions or boxes; a month-long record for a particular box spans an entire tape. (2) SFCOBS is an objective analysis of surface-based cloud observations over land and sea. The fractional cloud amount in the higher of two layers is derived from the reported fractional cloud amount in the lower layer and total cloud cover, assuming the clouds in the two layers randomly overlap. If three cloud layers are reported simultaneously, the respective cloud amounts are indeterminate, unless additional assumptions are made. Approximately 5% of all observations are rejected for this reason, compared to 10% for all quality control checks. As illustrated in Figure 3 of GHS, the data base on a typical day is extremely sparse over the oceans, especially in the tropics and southern hemisphere.

The data bases and method of reconstruction of the above analyses are discussed in more detail in GHS. Suffice it to say, the analyses of 3DNEPH and SFCOBS observed cloud amounts were interpolated to our spectral GCM's grid.

2.5. *Other Meteorological Data*

The relevant observed monthly mean or instantaneous meteorological initial conditions have to be provided to the GCM in order to evaluate the model-diagnosed radiative fluxes. The monthly mean temperature and wind fields for January 1977 and July 1979 are time-averaged National Meteorological Center (NMC) daily analyses interpolated to our GCM grid. The monthly mean water vapor field is obtained from an optimum interpolation analysis of temperature and dewpoint depression station data, using climatology as a first guess. Initial conditions for the January 1, 1977, and the June 10, 12, and 14, 1979, cases are provided by a GFDL

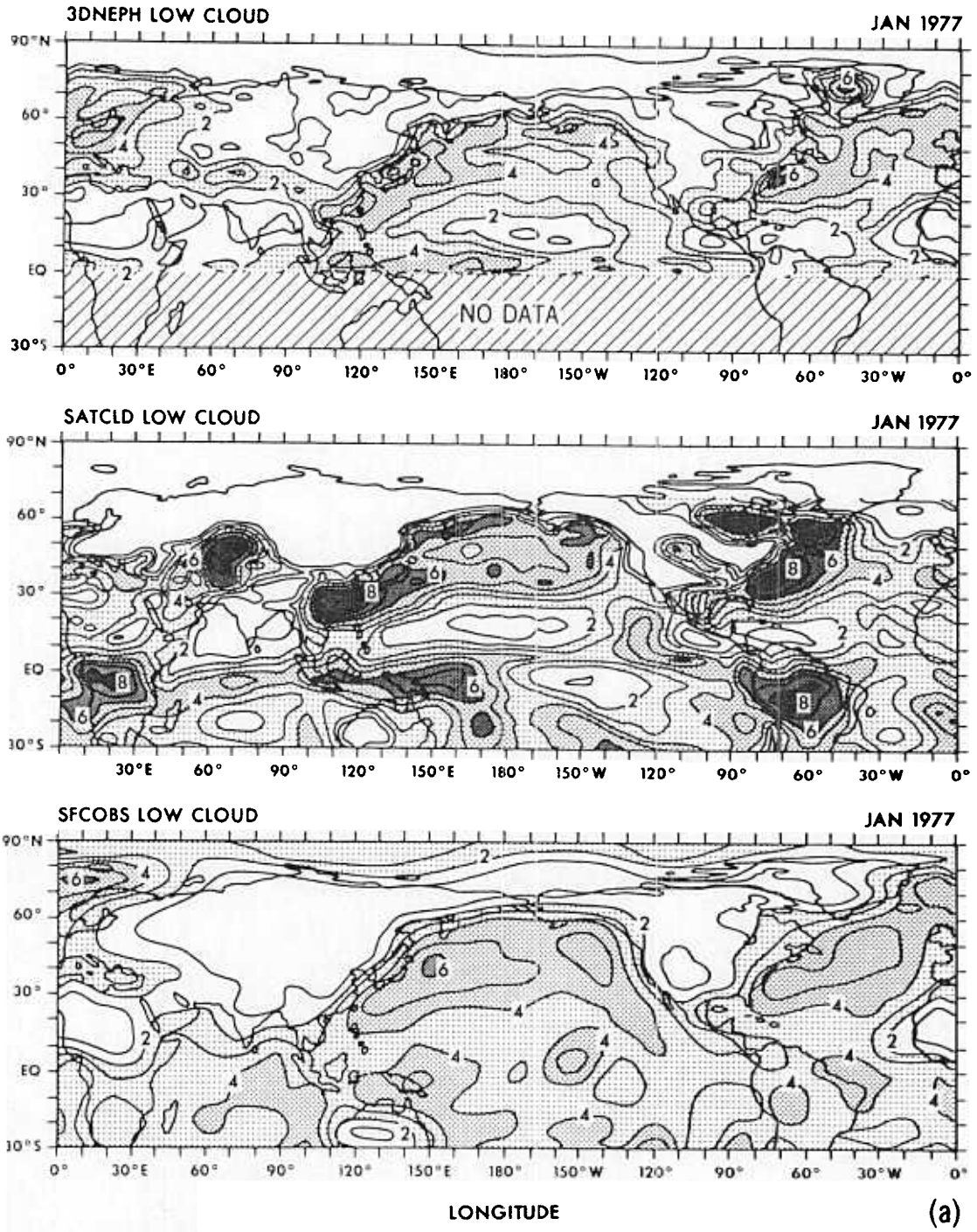

Fig. 2. Monthly mean analyses of cloud amount over the 90°N to 30°S domain for January 1977: (*a*) low clouds, (*b*) high clouds, (*c*) total clouds. Contour interval, 0.1. Stippling: 0.8–1.0 (very fine), 0.6–0.8 (fine), 0.4–0.6 (medium), 0.2–0.4 (coarse), 0–0.2 (none).

four-dimensional analysis. The scheme is similar to the one described by *Ploshay et al.* [1983].

Climatological monthly mean sea surface temperatures (interpolated from data supplied by the Scripps Institution of Oceanography) are specified over the open ocean. Meanwhile, for convenience, and to guarantee a model-consistent surface heat budget, the initial surface temperature T_s is, strictly speaking, model-predicted, rather than observed, over land and sea ice. The same procedure is used for medium- or long-range weather prediction experiments performed with our GCM. However, T_s should be rather constrained by the imposed observed vertical profiles of temperature, wind, and water vapor. Furthermore, over the oceans, these profiles are presumably influenced by the observed sea surface temperature field anyway. In any case the SATCLD effective cloud amount fields were found to be quite insensitive to whether (1) observed or climatological monthly mean sea surface temperature fields, which generally differed locally by less than 1 K or 2 K, were specified or (2) moist convective adjustment was turned on or off during the single time step integration.

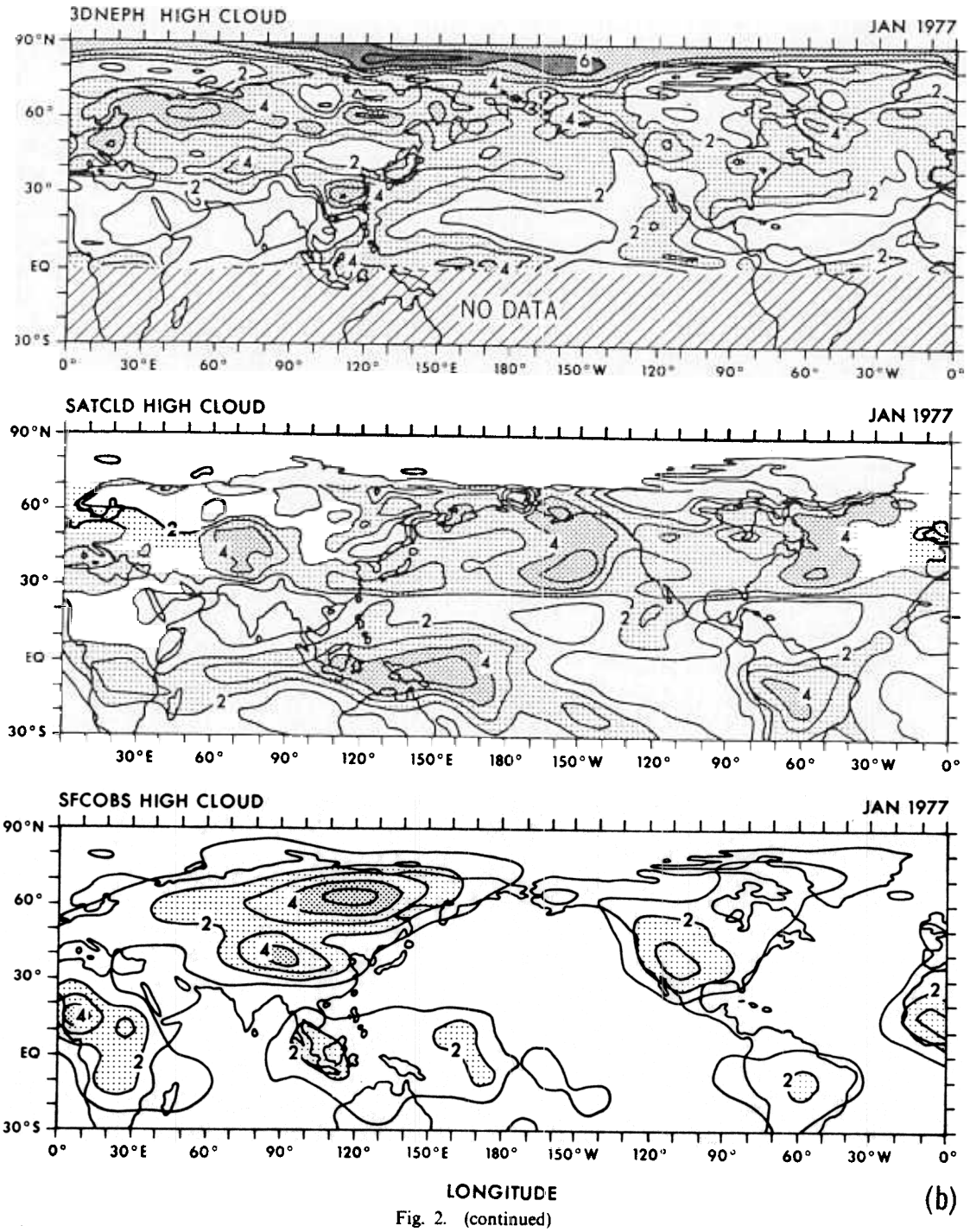

Fig. 2. (continued)

COMPARISON OF SATCLD EFFECTIVE CLOUD AMOUNT FIELDS WITH OBSERVED

To qualitatively assess the plausibility of the SATCLD effective cloud amount fields, a few comparisons are made with the 3DNEPH and SFCOBS analyses of observed cloud amount. The SATCLD-3DNEPH comparison is of primary concern since both rely extensively on satellite-derived data—from the same satellite during January 1977 and from different satellites in 1979. However, SFCOBS provides another perspective and is all we have to compare with south of the equator.

A quantitative verification of the SATCLD analyses of effective low and high cloud amounts is not possible for several reasons: (1) The "ground truth" is not accurately known. (2) The implied definitions of cloud amount are different for satellite-derived versus surface-based observations, as alluded to by GHS. (3) Only two effective cloud parameters, e.g., low and high cloud amount, could be derived from the two independent radiative flux parameters archived by NESDIS. In other words any middle clouds would be incorporated into low or high effective cloud amount by the SATCLD scheme. On the other hand the SFCOBS scheme cannot cope with three distinct layers of cloud existing simultaneously, whereas the AFGWC makes certain model assumptions to generate the vertical distribution of its 3DNEPH clouds. (4) The input data used to generate the SATCLD, 3DNEPH, and SFCOBS analyses of cloud amounts are not spatially or temporally

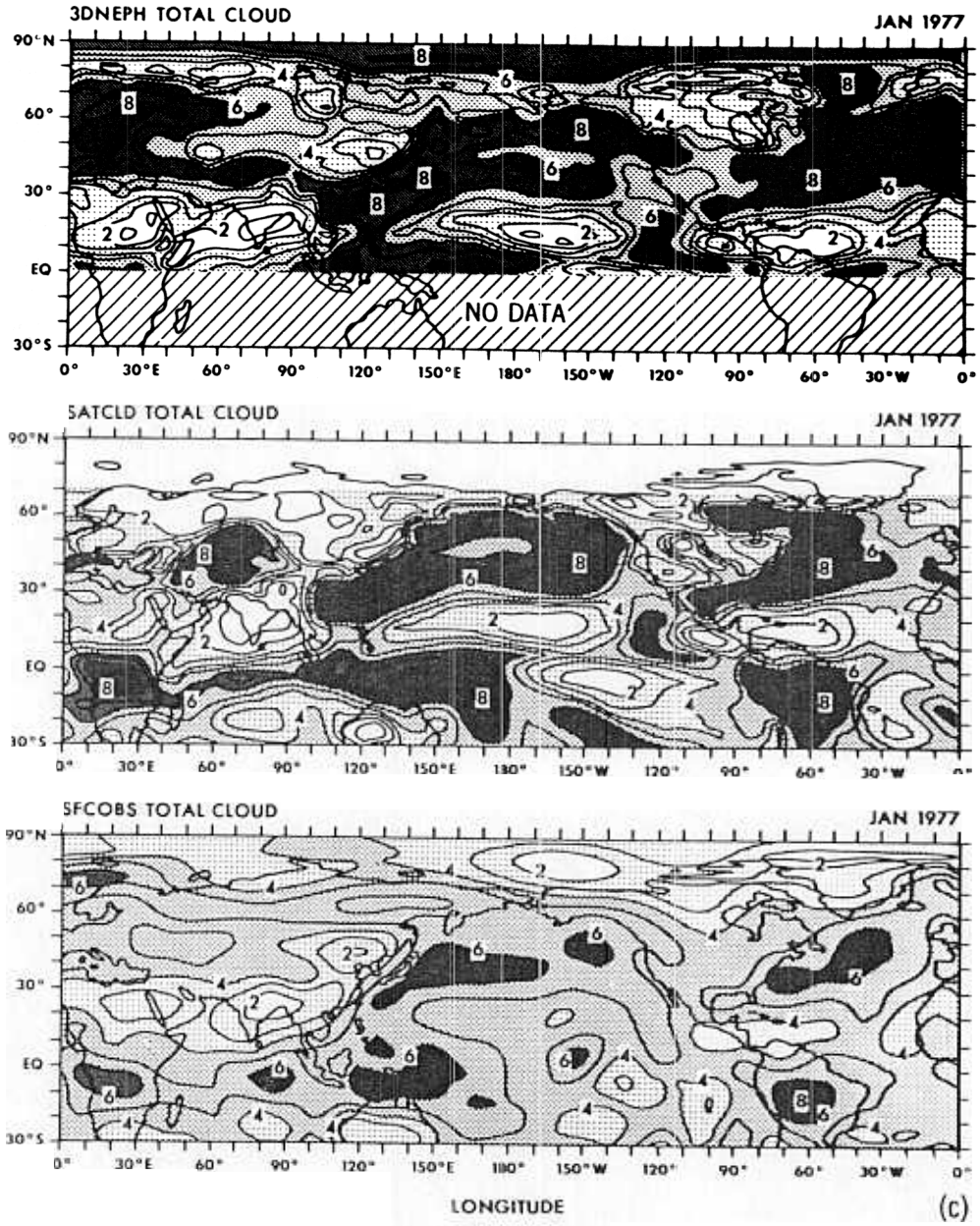

Fig. 2. (continued)

synchronized. Despite the above limitations, comparisons at face value can hopefully give some indication of whether various features of the SATCLD effective cloud amount fields are plausible.

For simplicity, both "effective cloud amount" and "observed cloud amount" will frequently be referred to as "cloud amount" from now on. However, the implied meaning should be obvious from the context of the discussion.

3.1. *Monthly Mean Results*

One reason for being interested in monthly means is the hope that monthly mean effective cloud amount fields could be specified, ultimately, in monthly/seasonal range GCM weather prediction experiments at GFDL.

Latitude-longitude maps of SATCLD, 3DNEPH, and SFCOBS analyses of monthly mean (*a*) low, (*b*) high and (*c*) total cloud amount for January 1977 and July 1979 are illustrated in Figures 2 and 3, respectively. The domain is restricted to 90°N to 30°S, since the SFCOBS analysis is not usable farther south. Also, note that the 3DNEPH analysis terminates at the equator. The January 1977 SATCLD analyses have been suppressed poleward of 70°N, where they are extremely noisy.

According to Figure 2*a*, the 3DNEPH, SFCOBS, and SATCLD analyses of low cloud amount n_l for January 1977 bear a qualitative resemblance over the mid-latitude oceans but not over the snow-covered Eurasian and North American continents poleward of 40°N, where the estimated surface albedo may be very inaccurate. In the polar night region the SATCLD n_l field (not shown) is very noisy for two reasons: First, equation (2) is not used to determine n_l, since $S_{obs} = 0$. Second, a small adjustment in F_{obs} may generate a large adjustment in n_l because the model-computed surface temperature T_s, the observed temperature at low cloud top level, and the effective emission temperature $T_e \propto F_{obs}^{1/4}$ are nearly the same. Over the Sahara Desert, SATCLD exhibits more low cloud than 3DNEPH or SFCOBS. Here, the specified surface albedo may be too low, as discussed below in connection with

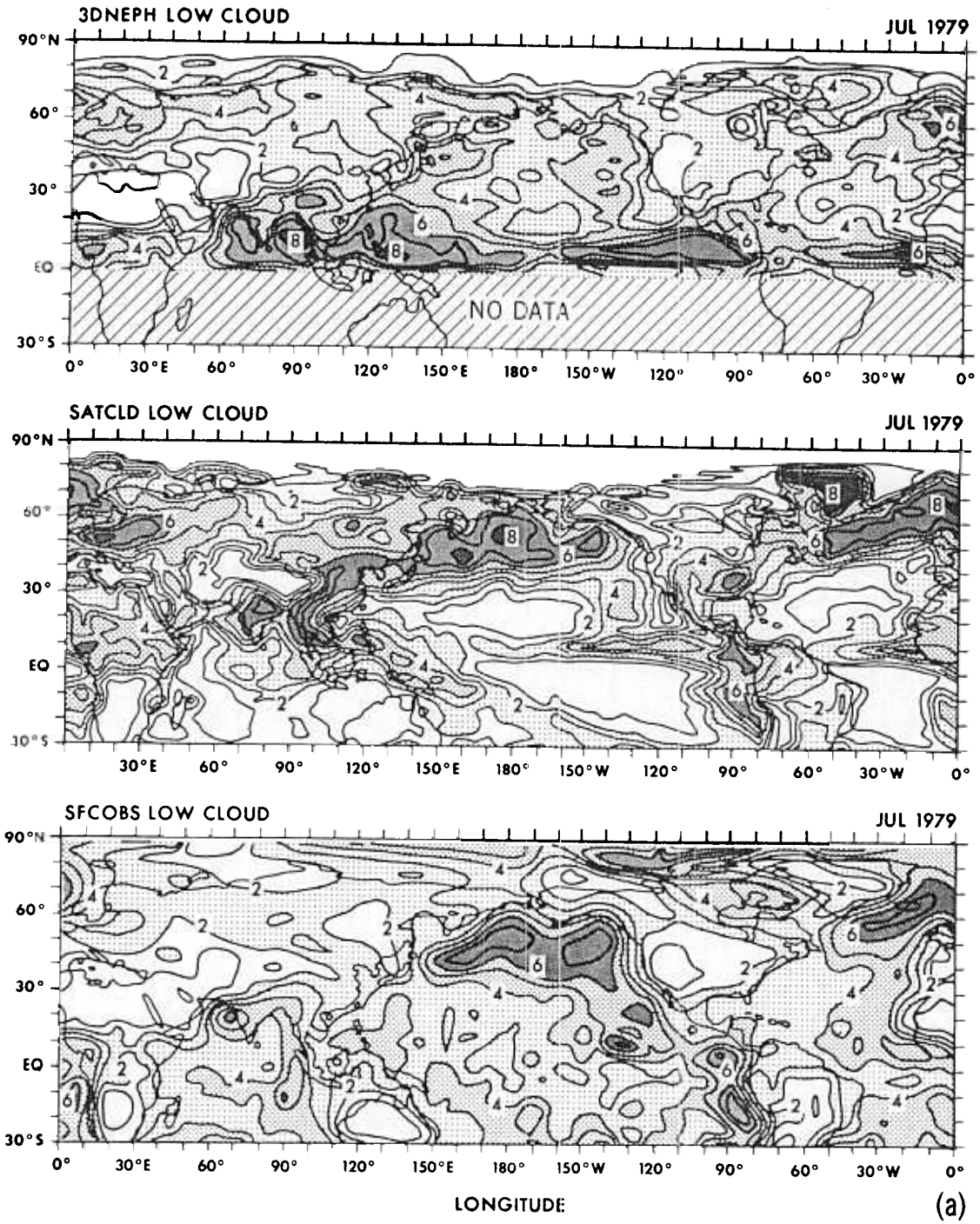

Fig. 3. Same as Figure 2, except for July 1979.

the July 1979 case. Over the subtropical and tropical oceans of the northern hemisphere, the two satellite-data-dependent analyses of n_l, both based upon NOAA 5 data, have more extreme minima than SFCOBS. Moreover, in the southern hemisphere tropics the SATCLD convergence zones are clearly more organized than the SFCOBS, especially over the south tropical Pacific, Brazil, and equatorial Africa. Notice the local maximum in SATCLD low cloud amount over the eastern Pacific Ocean, somewhat off the west coasts of Central and South America.

Generally speaking, the three analyses of high cloud amount n_h for January 1977 (Figure 2*b*) bear less resemblance than the corresponding analyses of n_l. The two satellite-based analyses of n_h are most similar, perhaps, over the northern hemisphere tropics. As at the lower level, the upper-level SATCLD South Pacific and Intertropical Convergence Zones (ITCZ) are much better defined than SFCOBS'.

During July 1979, the SATCLD n_l field resembles SFCOBS more closely than 3DNEPH over the north central Pacific and northeast Atlantic oceans (Figure 3*a*). Note that the SATCLD n_l ITCZ is quite well defined, whereas the 3DNEPH is (for currently unexplained reasons) more intense, and the SFCOBS ITCZ is again fragmented or nonexistent over data-sparse regions. Meanwhile, SATCLD clouds resemble stratus

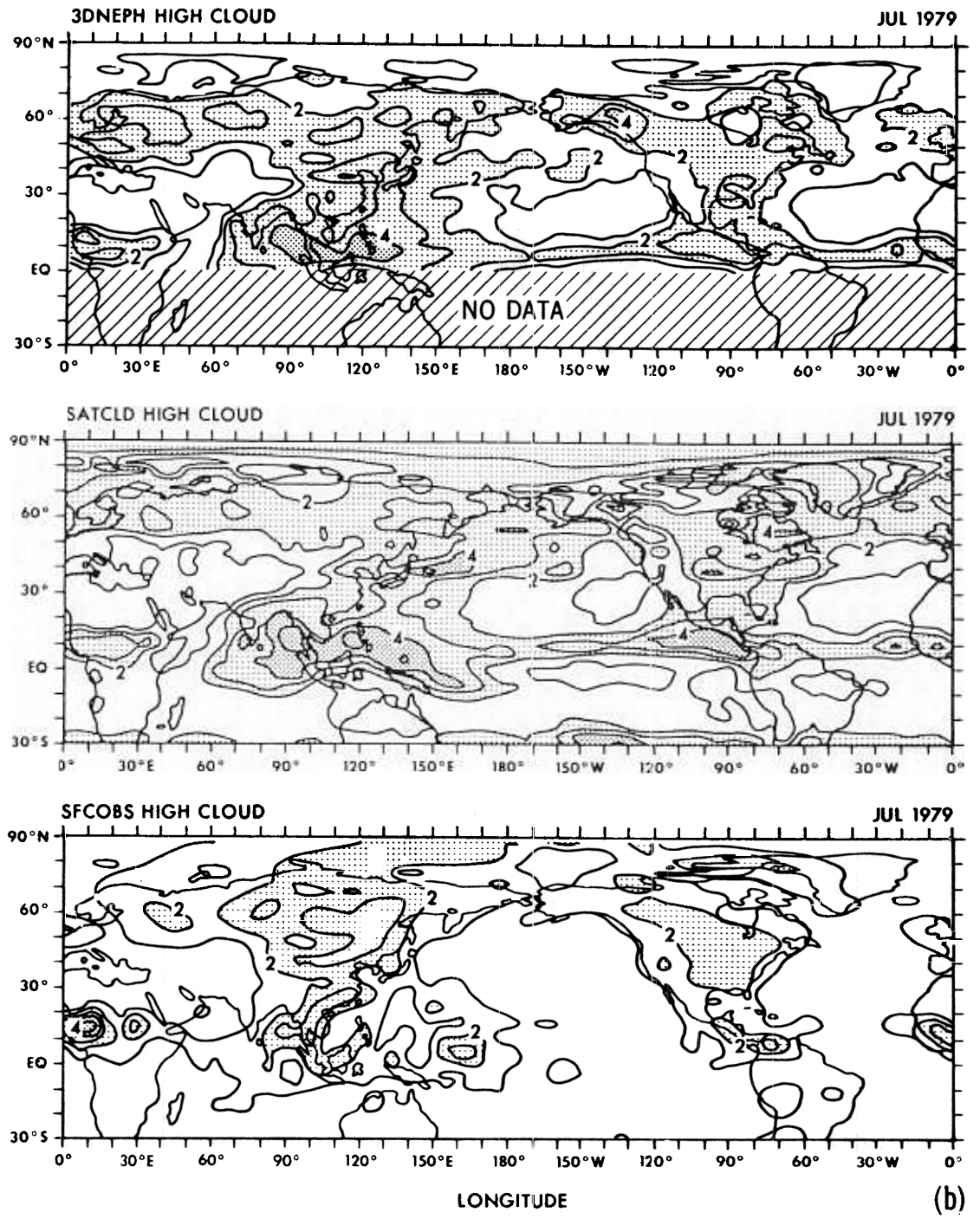

Fig. 3. (continued)

or stratocumulus, i.e., n_l attains a relative maximum (Figure 3*a*) and $n_h \sim 0$ (Figure 3*b*) off the west coasts of southern Africa and South America, in qualitative agreement with SFCOBS.

The SATCLD maximum in n_l over the southeastern United States is more pronounced than the 3DNEPH or SFCOBS. Similarly, the prominent SATCLD dry zones in the west central subtropical Pacific and subtropical Atlantic oceans are not found in the other two analyses. Unfortunately, comparable digitized DMSP radiative flux data, which might help to sort out the true causes of these SATCLD-3DNEPH discrepancies, were not available. However, we speculate that two possible causes are the incorporation of timely surface-based observations of clouds into the AFGWC 3DNEPH analysis and systematic differences between TIROS-N versus DMSP satellite data. In support of the latter hypothesis the 3DNEPH and SATCLD analyses of n_l over the subtropical east central Pacific were more similar in January 1977, when both employed data from the same satellite. Regarding differences in the July 1979 satellite data, spectral reflectance is measured in the early morning, early evening, and around noon local time by the two DMSP satellites, but only once per day in the midafternoon, i.e., at 1500 hours by TIROS-N. Furthermore, the DMSP visible band (0.4–1.1 μm) is somewhat broader than the corresponding TIROS-N band (0.50–0.93 μm). Perhaps, the amount of low clouds, and hence the reflected solar radiation over the subtropical east central Pacific, approaches a minimum during the midafternoon. (Such

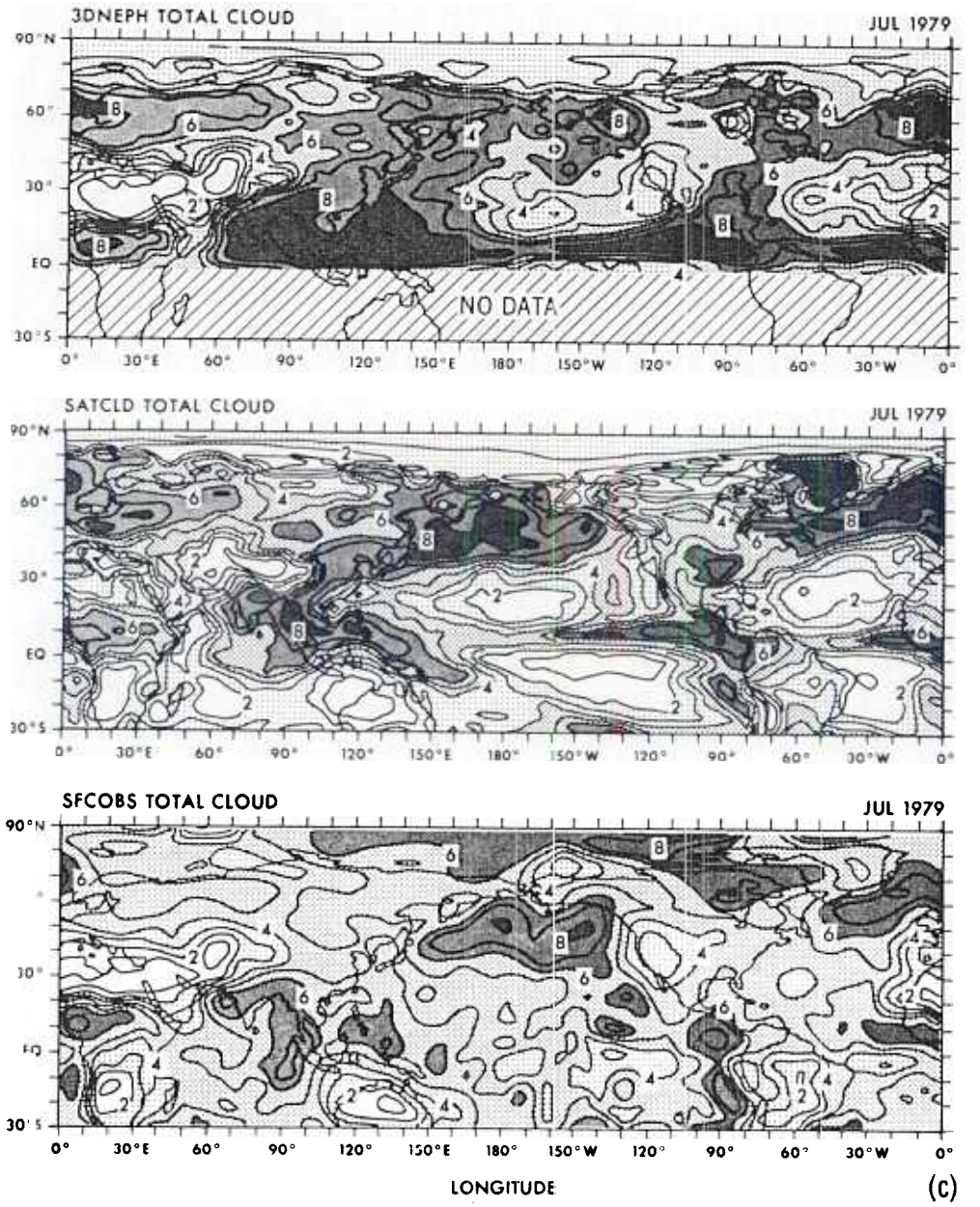

Fig. 3. (continued)

behavior has been noted by *Minnis and Harrison* [1984] off the west coast of South America in their recent analysis of November 1978 GOES satellite data.) Conversely, over the southeastern United States, thermal convection may be approaching its diurnal maximum intensity during the midafternoon. The existence of a relative maximum of SATCLD high cloud amount (see Figure 3*b*) at the same location is suggestive of deep convection.

A negative bias in the specified surface albedo field may also enhance the SATCLD n_1 maximum over the southeastern United States. We assumed $A_s \sim 0.08$ over the southeastern United States. But according to the CLIMAP (Climate: Long-Range Investigation, Mapping, and Prediction) analysis (obtained from Bruce Grant, NOAA, Boulder, Colorado 80302, 1981), $A_s \sim 0.16$. If this latter estimate were adopted, SATCLD n_1 would decrease locally by ~ 0.1. Similarly, the surprisingly large amount of SATCLD n_1 over the Sahara Desert may compensate for a negative bias in our specification of the surface albedo and/or neglect of scattering by Sahara dust. The CLIMAP values of A_s there are 0.03–0.10 greater than ours. Meanwhile, the virtual absence of SATCLD low clouds over the permanently snow-covered Arctic region suggests that the currently assumed value of A_s for July, i.e., 0.75, is too high, perhaps because of our neglect of snowmelt.

To test the sensitivity of our results to an improved specification of surface albedo, SATCLD effective clouds were recalculated using the CLIMAP surface albedo field and including a surface-temperature-dependent parameterization of A_s over melting snow. The latter parameterization is similar to *Robock*'s [1980] but less extreme. It reduced A_s over snow-covered land in the summer Arctic to ~ 0.55. The standard July surface albedo field A_s and the (new minus old) difference field ΔA_s are illustrated in Figures 4*a* and 4*b*, and the new SATCLD n_1 field in Figure 5. Given the new A_s field, n_1 decreases slightly over the southeastern United States, decreases over the Sahara, and increases over the permanent Arctic snow pack.

The main point regarding the July 1979 fields of high cloud

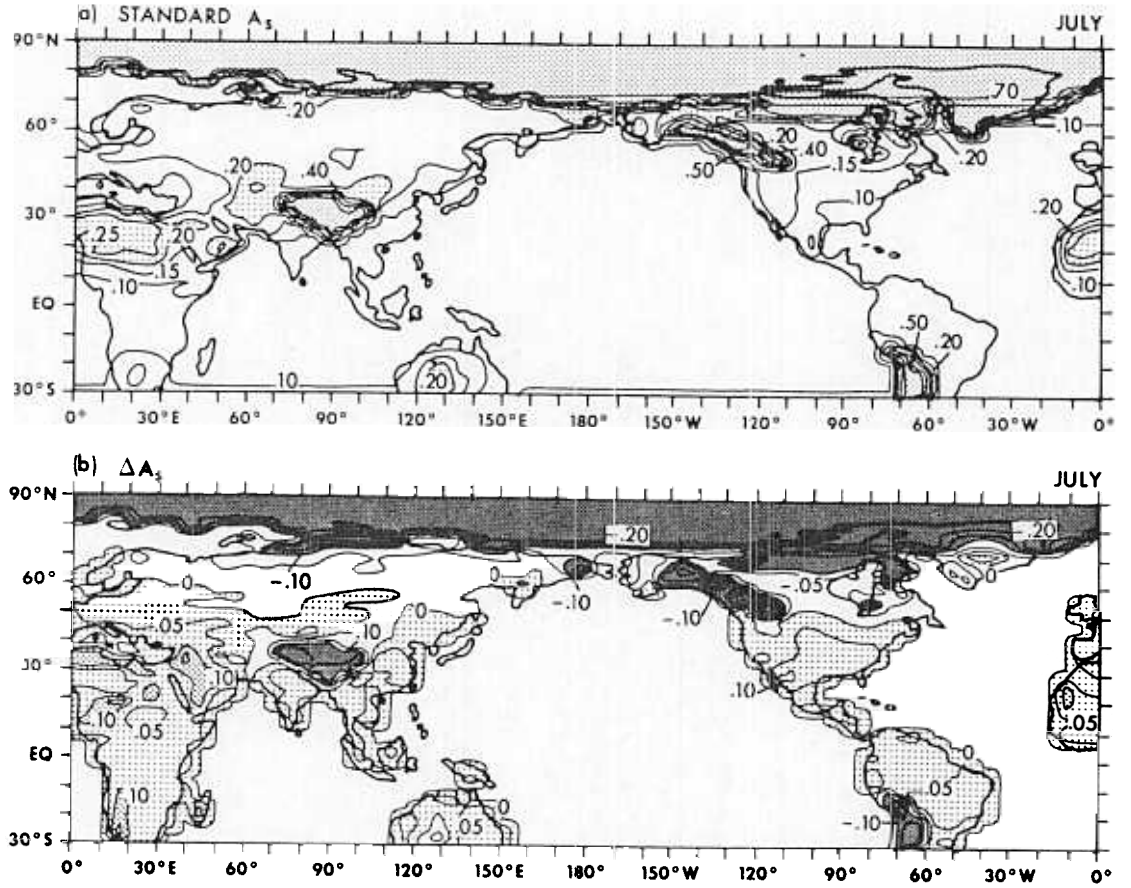

Fig. 4. Surface albedo fields for July 1979: (*a*) standard surface albedo A_s; contour interval, 0.05 or 0.10; light stippling for $0.20 \leq A_s \leq 0.40$, darker stippling for $A_s > 0.40$; (*b*) differential, i.e., new minus standard surface albedo ΔA_s; contour interval, 0.05; light stippling for $0 \leq \Delta A_s \leq 0.10$, medium stippling for $\Delta A_s > 0.10$, dark stippling for $\Delta A_s < -0.10$.

amount n_h (Figure 3*b*) is that SATCLD and 3DNEPH are in qualitative agreement over both the extratropics and tropics. In particular, their ITCZ's are much better defined than SFCOBS.

Analyses of total cloud amount N_T for January 1977 and July 1979 are illustrated in Figures 2*c* and 3*c*, respectively. The SATCLD field was derived under the assumption of random overlap, i.e., according to the formula $N_T = n_l + (1 - n_l)n_h$. The N_T fields incorporate various features of the corresponding n_l and, to a lesser extent, n_h fields. Note the similarity in structure of the 3DNEPH and SATCLD N_T fields in the tropics and subtropics (excluding the Sahara).

Latitudinal profiles of zonal mean ("$\langle\ \rangle$") SATCLD and 3DNEPH cloud amounts are plotted for January 1977 (Figure 6) and July 1979 (Figure 7). The $\langle n_l \rangle_{SATCLD} - \langle n_l \rangle_{3DNEPH}$ difference is generally positive in the northern hemisphere winter or summer extratropical cyclone belts and quiescent January northern hemisphere tropics. In contrast it is negative in the summer northern hemisphere tropics, approaching 0.20 in the ITCZ. Meanwhile, the SATCLD and 3DNEPH profiles of

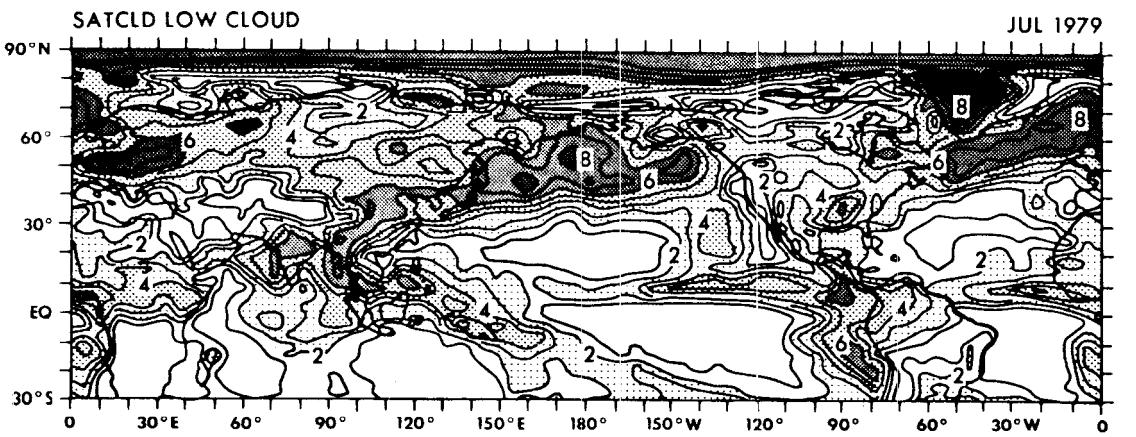

Fig. 5. SATCLD low cloud amount field corresponding to new surface albedo, for July 1979. Contour intervals and stippling are the same as in Figure 2*a*.

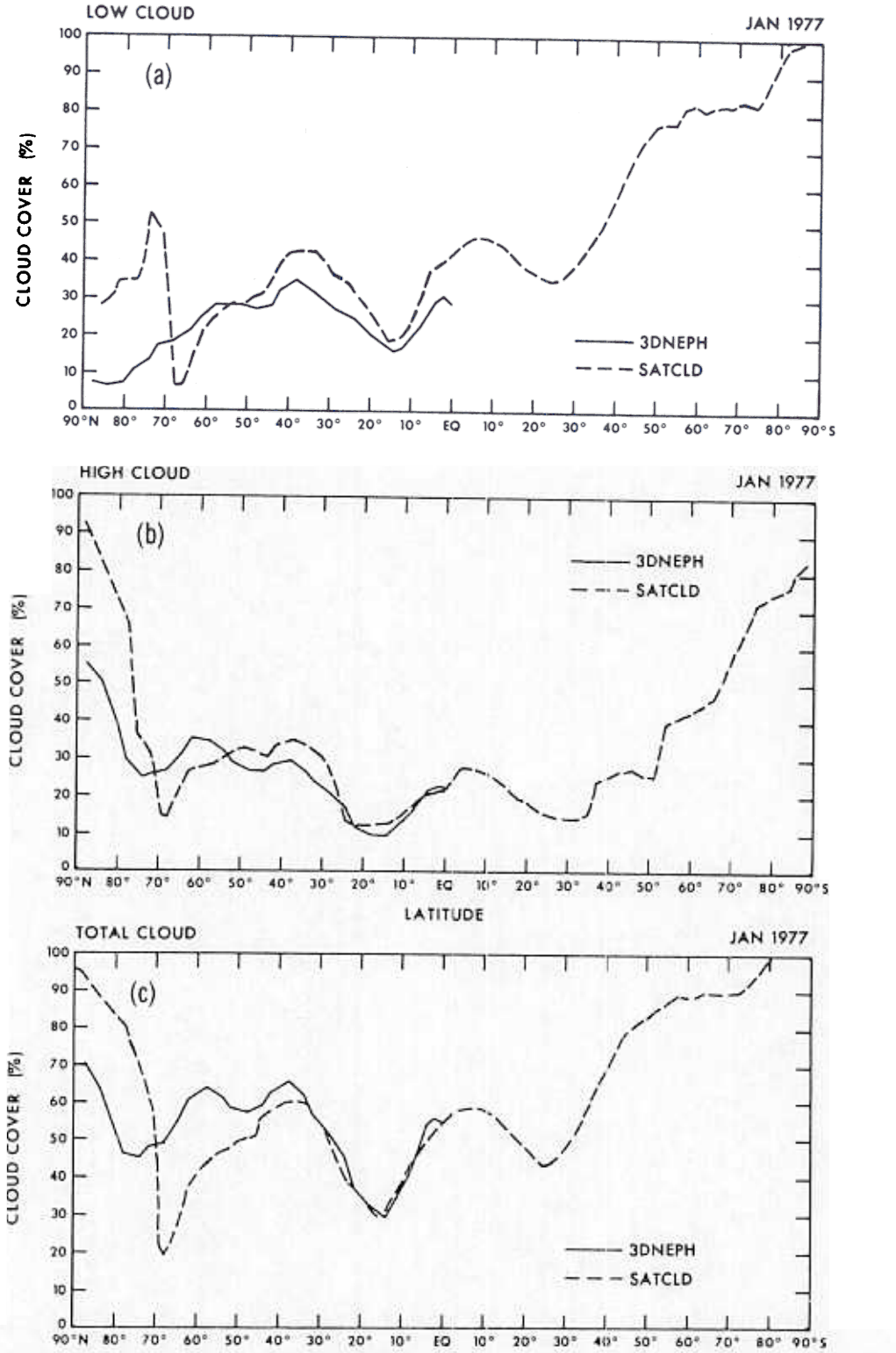

Fig. 6. Latitudinal profiles of zonal mean monthly mean cloud amount for January 1977: (*a*) low clouds; (*b*) high clouds (*c*) total clouds. The domain is 90°N to 90°S.

$\langle n_h \rangle$ are remarkably similar equatorward of 60°N. The agreement between the two $\langle N_T \rangle$ profiles in the mid-latitudes is enhanced by the compensating contribution of $\langle n_m \rangle_{3DNEPH}$.

As shown in Figure 7, the SATCLD scheme generates a low overcast within the 45°S to 60°S latitude belt in July 1979. Further analysis indicated that this result is related to an inconsistency between model-diagnosed zonal mean absorbed shortwave radiative flux (16 W m^{-2}) versus observed (2 W m^{-2}). The true observed value was apparently underestimated by NESDIS. First of all, in their conversion of instantaneous reflectivities to diurnal mean values, they did not take proper account of zenith angle dependence, although the local zenith angle was very large at 1500 hours local time. More generally, the effects of bidirectional reflectance were not incorporated

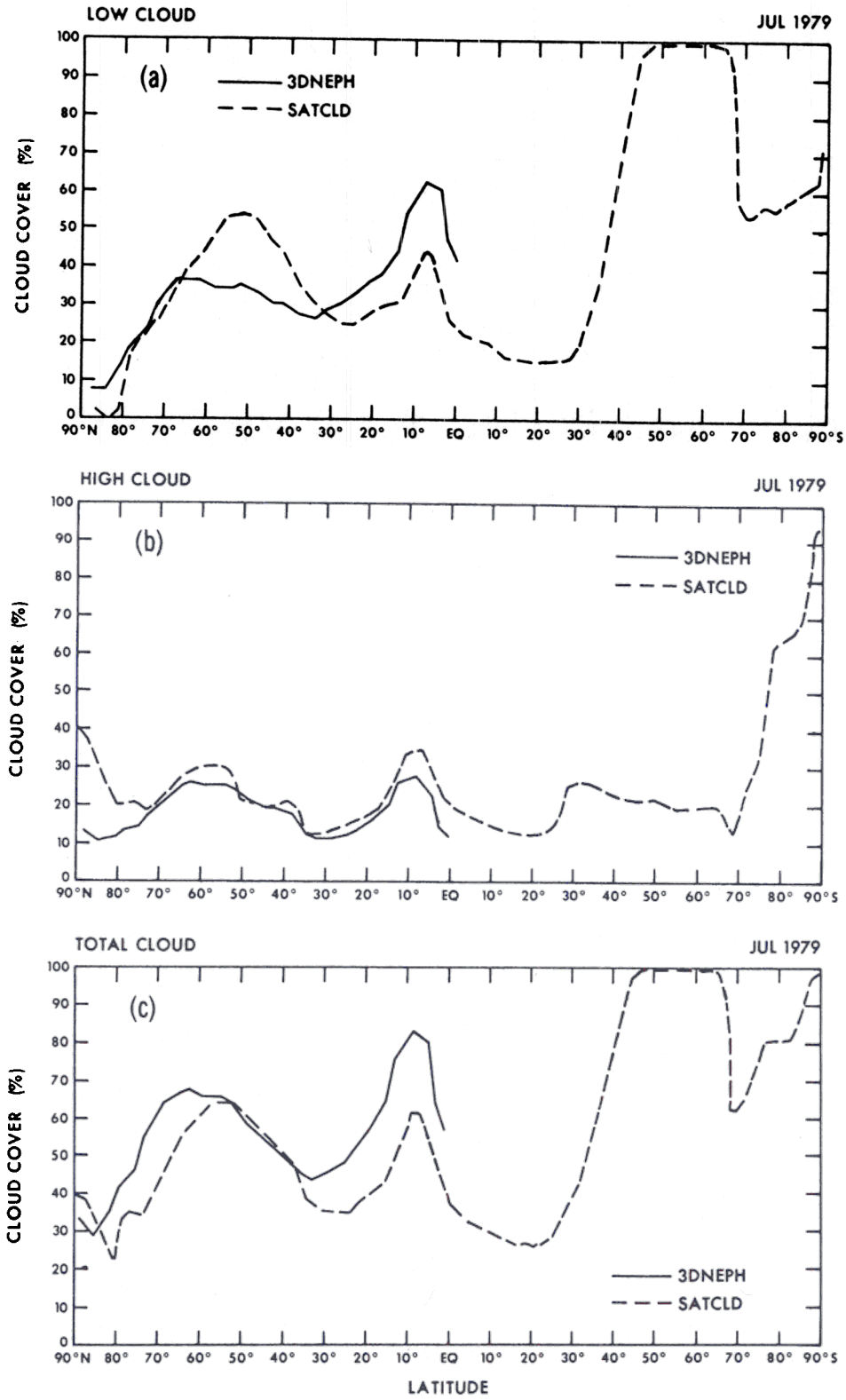

Fig. 7. Same as Figure 6, except for July 1979.

into their data processing scheme. In contrast, zenith-angle-dependent anisotropic correction factors, developed by *Taylor and Stowe* [1984], have been applied to Nimbus 7 satellite data.

SATCLD and 3DNEPH northern hemispheric monthly mean values of n_l, n_m, n_h, and N_T are summarized in Table 2. There is substantial 3DNEPH middle-level cloud and slightly less high-level cloud compared to SATCLD.

Although the sensitivity of the SATCLD effective high cloud amount to cloud top height was not systematically investigated, some information was obtained inadvertently when an erroneous "observed" temperature profile $T(\sigma_{l+1})$ was

specified instead of $T(\sigma_1)$ in the upper troposphere: $0.189 \leq \sigma_1 \leq 0.500$. (Here, σ_1 is the vertical coordinate pressure over surface pressure at GCM level 1). A 15 K positive bias in $T(0.189)$ resulted that was equivalent to lowering the high clouds in the tropics from ~189 mbar to ~336 mbar. The phase of the corresponding n_h fields remained similar to that of Figures 2*b* or 3*b*. However, the amplitude of n_h increased substantially in the tropics, e.g., by over 50% in relative terms within the July 1979 ITCZ. Conversely, n_l decreased by up to 0.1 to compensate for the enhanced reflection of shortwave radiation by n_h. Incidentally, the use of uncorrected NESDIS long-wave flux data elicited a somewhat weaker response of opposite sign.

3.2. *Daily Mean Results*

For some GCM applications, e.g., when the transient activity is strong, daily varying specified cloud amount fields may be of interest. Therefore we decided to test whether the SATCLD scheme can generate plausible yet radiatively consistent distributions of effective cloud amount on this time scale. The example of January 1, 1977, the only one for which we have both SATCLD and 3DNEPH analyses, is emphasized here. SFCOBS is excluded from the comparison, since that analysis for a particular day would suffer from tremendous data gaps over the oceans, tropics, and southern hemisphere. Note that the partial derivatives of equations (1) and (2) now correspond to observed meteorological conditions on January 1, 1977, 0000 GMT.

The SATCLD and 3DNEPH fields of N_T for January 1, 1977, are shown in Figure 8. Although both analyses are asynoptic, the 3DNEPH is somewhat smoother. The background synoptic analyses of 500-mbar and 1000-mbar geopotential height and 850-mbar temperature for January 1, 1977, 1200 GMT, are plotted in Figures 9*a*, 9*b*, and 9*c*, respectively.

Overall, the two fields of total cloud amount are quite similar, despite some discrepancies. The large spiral of cloud over the North Pacific is associated with an intense disturbance. The cloud bands that straddle the east coasts of Asia and North America are apparently due to the advection of cold air over relatively warm water. Several large-scale features in the N_T fields are recognizable in the n_l and n_h fields (not shown) as well.

Over the upper Great Lakes, Scandinavia, and the western part of the Soviet Union, the 3DNEPH is more consistent with surface synoptic reports of cloud cover (not shown). Two factors may be relevant here. First, timely surface observations of cloud amount are utilized by the AFGWC 3DNEPH analysis. Second, a serious attempt is made by the AFGWC to discriminate between cloud cover and snow cover. More precisely, satellite shortwave radiative flux data is compared against an evolving background brightness field. Although the surface albedo for the SATCLD calculations depended upon snow depth d, only weekly mean values of d were utilized. Furthermore, other factors, previously mentioned in section 1, that influence the albedo over snow-covered land were neglected.

As a second example, SATCLD effective clouds (but not 3DNEPH) were generated for June 10, 12, and 14, 1979. The SATCLD analyses (not shown) appeared to simulate the rapid onset of the summer Indian monsoon. A prominent feature, i.e., two distinct regions of cloudiness over the Arabian Sea and Bay of Bengal on June 14 are consistent with streamline analyses at 850 and 200 mbar as well as satellite photographs.

TABLE 2. Northern Hemispheric Monthly Mean Cloud Amount

Case	Layer	3DNEPH	SATCLD
January 1977		0.218	0.244
		0.196	0.000
		0.249	0.308
		0.503	0.465
July 1979	High	0.187	0.222
	Middle	0.251	0.000
	Low	0.376	0.342
	Total	0.587	0.474

4. Radiative Consistency of Model-Diagnosed Fluxes

SATCLD model-diagnosed radiative fluxes were calculated by our spectral GCM from observed meteorological data, primarily to confirm whether they are really consistent with observation. At first glance, consistency seems assured, barring errors in the computer code or inaccurate Taylor series approximations to S_{obs} and F_{obs}. However, substantial discrepancies could occur locally where GCM-dependent biases and/or observation-dependent biases are "sufficiently large" to activate the physical realizability constraints, i.e., equations (4*a*) and (4*b*). Thus some qualitative information may be inferred about robust GCM-dependent and/or observation-dependent biases by examining model-diagnosed SATCLD fluxes.

GCM-diagnosed radiative fluxes corresponding to "alien" observed clouds (mainly the satellite-data-dependent 3DNEPH) are also illustrated. Our purpose is to simply demonstrate that the discrepancies from observation are indeed larger, overall, for such clouds than for SATCLD effective clouds. In the case of 3DNEPH clouds the discrepancies could emerge as a result of (1) deficiencies in the AFGWC 3D-Neph analysis; (2) deficiencies in our own GCM's cloud radiation model, treatment of surface albedo, and/or treatment of aerosols; or (3) discrepancies between DMSP versus NOAA satellite data. However, more accurate and comprehensive data sets would be needed to quantitatively estimate the contributions of these factors. Thus the present intercomparison of GCM-diagnosed versus observed radiative fluxes should not be viewed as a verification of observed or effective cloud amount fields. Admittedly, the use of improved input and verification data could alter the results. Also, the 3DNEPH (and SFCOBS) fluxes are at a disadvantage, since the "observed" fluxes employed by the SATCLD analysis scheme also serve as the verification data. But in the January 1977 cases at least, the 3DNEPH and SATCLD analyses are based upon radiance data measured by the same satellite, i.e., NOAA 5.

SATCLD and 3DNEPH model-diagnosed fields of outgoing long-wave flux F, reflected shortwave flux $S\uparrow$, and net flux R have been compared with observation (Winston OBS). Maps of the July 1979 monthly mean F and $S\uparrow$ fields are illustrated in Figures 10*a* and 10*b*, respectively. As anticipated for SATCLD clouds, all three model-diagnosed flux fields in the tropics and summer extratropics correspond very well with January 1977 or July 1979 monthly mean satellite verification data. In those regions, even the January and July 3DNEPH long-wave flux fields essentially reproduce the longitudinal variation of the observed. These results are consistent with the qualitative similarity between the 3DNEPH versus SATCLD fields of high cloud amount. In contrast the 3DNEPH $S\uparrow$ and (hence the R) flux field deviates substantially

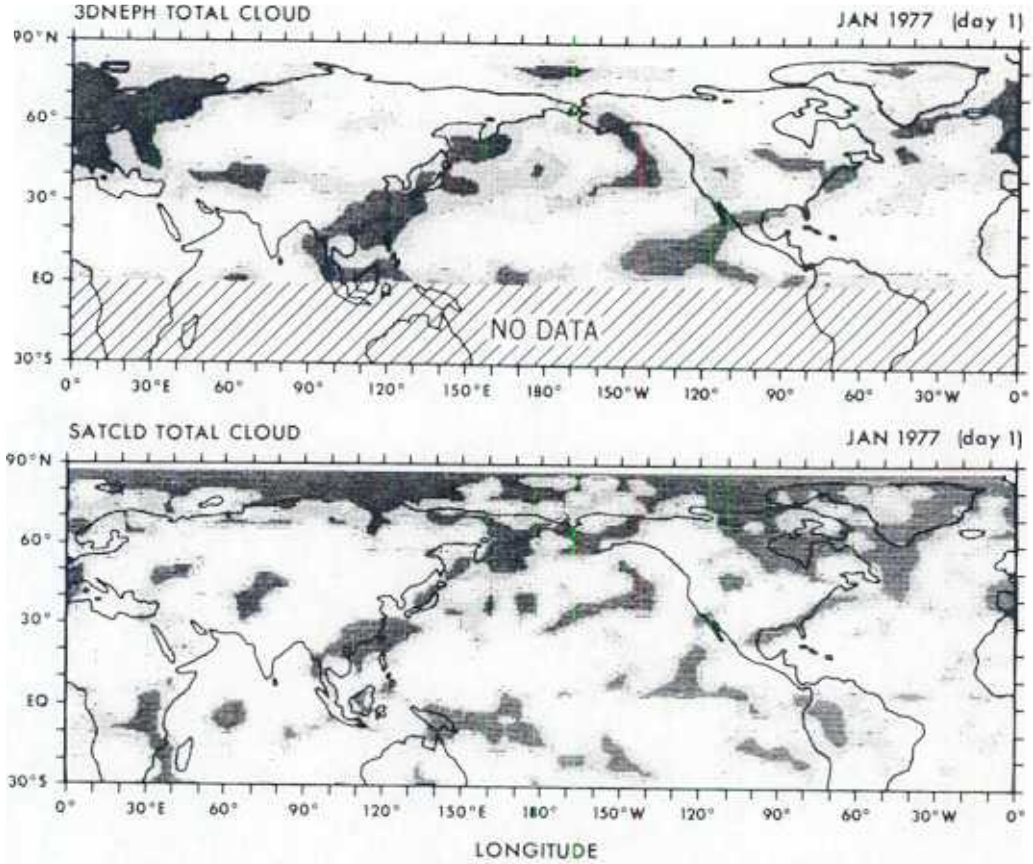

Fig. 8. Same as Figure 2c, except for January 1, 1977, SATCLD and 3DNEPH clouds, with contours suppressed

from SATCLD over the central tropical and subtropical oceans, especially in July 1979. In fact the 3DNEPH clouds appear to reflect up to 50 W m^{-2} more solar radiation to space over the eastern Pacific section of the July 1979 ITCZ and over the 15°N to 30°N latitude belt of the east central Pacific. These latter results are consistent with the locally greater amounts of 3DNEPH low cloud. Meanwhile, in the winter extratropics, S is small compared to F, whereas F and hence the net flux R are relatively insensitive to cloud amount, being controlled more by the land-sea contrast in surface temperature.

Model-diagnosed and observed eddy radiative fluxes, i.e., the departures from their respective zonal means, were cross correlated along each Gaussian latitude, and the correlation coefficients $r(F)$, $r(S)$, and $r(R)$ plotted versus latitude. In the January monthly mean case, typical values of $r(F)$ and $r(S)$ in the northern hemisphere tropics (not shown) are ~ 0.98 and ~ 0.98 for SATCLD clouds versus ~ 0.8 and ~ 0.6 for 3DNEPH. The January 1977 monthly mean as well as January 1, 1977, correlations $r(R)$ (Figure 11) remain high in the tropics for SATCLD but drop off sharply for 3DNEPH (and SFCOBS). Note that $r(R)$ may be more sensitive than $r(F)$ and $r(S)$ in the tropics, since $|R| \ll |F|$, and $|R| \ll |S|$ there. In the winter extratropics, $r(R)$ attains high values during January 1977, irrespective of whether SATCLD or 3DNEPH cloud amount fields are specified.

Although the radiative consistency of the SATCLD effective clouds is not merely an artifact of monthly time averaging, the January 1, 1977, daily SATCLD long-wave, and hence net radiative flux, correlation is somewhat weaker than the corresponding monthly mean correlation. A plausible explanation is that the satellite radiance measurements are not temporally synchronized with the model-diagnosed fluxes, which were calculated from the diurnal mean of the 0000 and 1200 GMT synoptic analyses of temperature. Discrepancies between F_{SATCLD} and F_{obs} are apt to be larger on a daily basis than on a monthly mean basis. They may be accentuated in regions of large diurnal variation and high maximum of surface temperature, e.g., the Sahara Desert in summer (see Figure 10*a*), if the satellite's daytime passage occurs near the time of diurnal maximum temperature, as in July 1979. In any case the lack of temporal synchronization between the "observed" temperatures input into the GCM versus those seen by the satellites cannot fully explain why the 3DNEPH correlations in Figure 11 are so much weaker.

Latitudinal profiles of differences, ΔR, between model-diagnosed and observed zonal mean net radiative fluxes for July 1979 are illustrated in Figure 12. The large 3DNEPH discrepancy near 50°N is an example of GCM cloud radiation model effects. The 3DNEPH (or SFCOBS) middle clouds apparently compensate for the relatively smaller fraction of low cloud amount so far as total cloud amount is concerned (see Figure 7). But they are unable to fully compensate radiatively, given our GCM's cloud radiation model, which assigns weaker albedos to middle clouds than to low clouds (see Table 1). Perhaps stronger middle-cloud albedos would be appropriate for cloud systems associated with intense mid-latitude transient synoptic disturbances. Not surprisingly, in the tropics, as elsewhere, $|\Delta R|$ is typically ≤ 5 W m^{-2} for SATCLD clouds. But there are two exceptions. First, $\Delta R \sim +15$ W m^{-2} in the 50°S to 60°S latitude belt (not shown), primarily because of the neglect of zenith-angle-dependent bidirectional

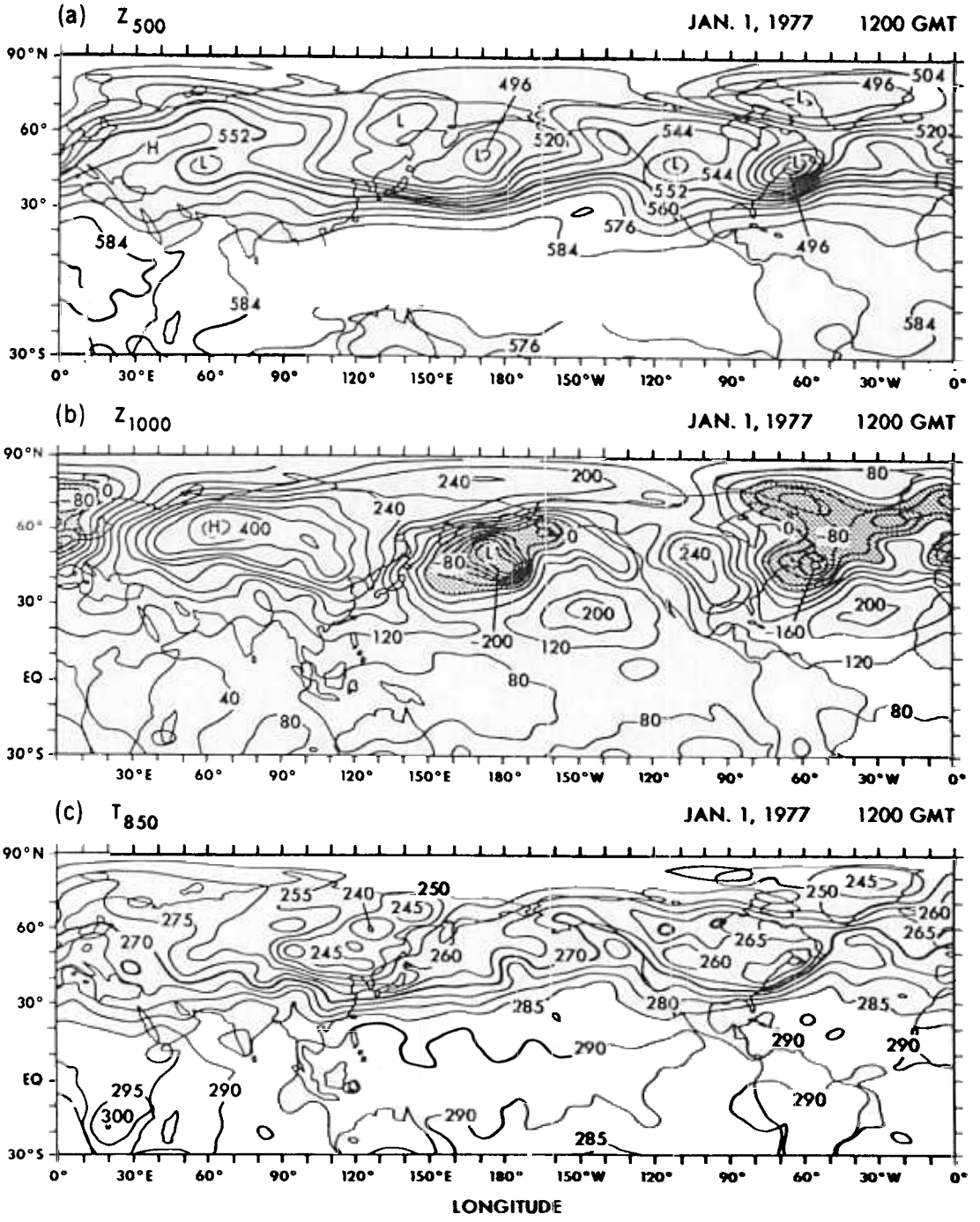

Fig. 9. Analyses of observed (*a*) 500-mbar geopotential height, (*b*) 1000-mbar geopotential height, and (*c*) 850-mbar temperature over the 90°N to 30°S domain for January 1, 1977, at 1200 GMT. Contour intervals in panels *a*, *b*, and *c* are 80 dam, 40 dam, and 5 K, respectively. Reference contours in panels *a* and *c* are 552 dam and 270 K. Stippling in *b* indicates negative heights.

reflectance in the conversion of instantaneous reflectivity measurements by NESDIS to diurnal mean broadband reflectivities. Second, $\Delta R \sim -45$ W m^{-2} in the Arctic, partly because of neglect of snowmelt in our standard surface albedo model and again partly because of NESDIS' neglect of bidirectional reflectance.

The atmospheric net radiative cooling and surface radiation balance are the direct links between cloud radiation and dynamics in GCM's. So, out of curiosity we have examined the sensitivity of vertical profiles of zonal mean net radiative cooling and surface net radiative flux to SATCLD versus 3DNEPH clouds. But unfortunately, no global or hemispheric observed data sets were available to verify these model-diagnosed radiative parameters.

The sensitivity of model-diagnosed vertical profiles of zonal mean net radiative cooling to the various analyses of cloud amount is most pronounced in the ITCZ. The situation for July 1979 and latitude 8°N is illustrated in Figure 13, where "London" refers to a zonal mean climatology of low, middle, and high cloud amount adapted from the northern and southern hemisphere climatologies of *Telegadas and London* [1954] and *Sasamori et al.* [1972], respectively. The 3DNEPH mid-

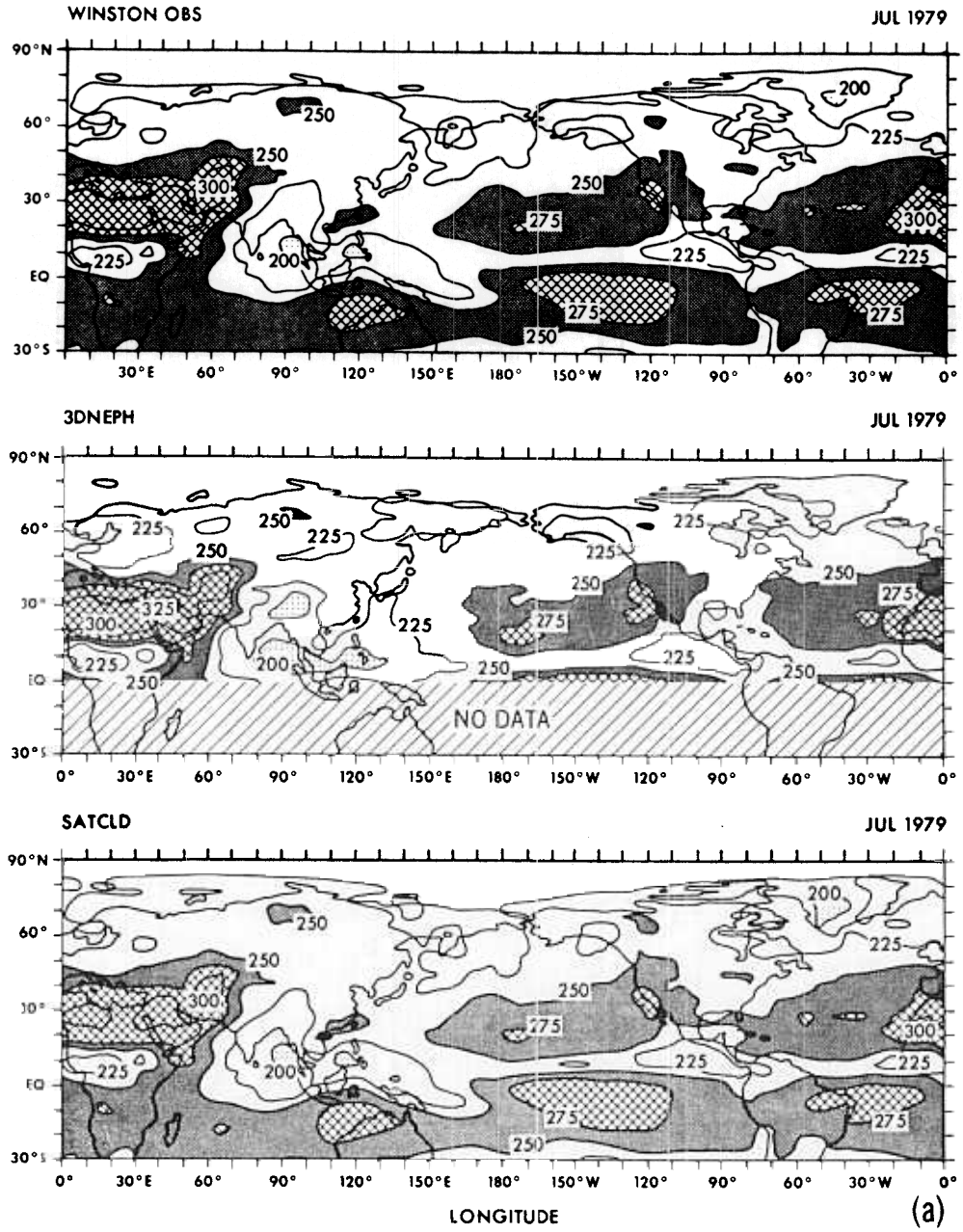

Fig. 10. Observed, and 3DNEPH and SATCLD model-diagnosed, radiative flux fields for July 1979: (*a*) outgoing long-wave and (*b*) reflected shortwave flux. The domain is 90°N to 30°S. Contour interval, 25 W m^{-2}.

tropospheric cooling is substantially greater than the SATCLD. Also, the 3DNEPH clouds tend to destabilize the lapse rate between $\sigma = 0.665$ and 0.500, whereas the SATCLD effective clouds tend to stabilize it. The discrepancy is attributed to the lack of SATCLD middle-level cloud. In comparison the 3DNEPH zonal mean cloud amount at $\sigma = 0.500$ and 8°N is $\langle n_m \rangle = 0.39$. SFCOBS and London mid-tropospheric net radiative cooling rates lie somewhere between the 3DNEPH and SATCLD values. The greater amount of 3DNEPH low cloud is responsible for the comparatively weaker 3DNEPH net radiative cooling in the lower tropical troposphere.

Thick convective clouds with high cloud tops may be more prevalent in the ITCZ than two or three distinct cloud layers. To simulate this situation, one thick layer of SATCLD clouds was generated, assuming the same base as for low clouds and the same top as for high clouds. For example, at 8°N the cloud top and cloud base were located at $\sigma = 0.336$ and $\sigma = 0.811$, respectively. As illustrated in Figure 13 these "convective" SATCLD effective clouds yield a strikingly different net radiative cooling profile at 8°N compared to the two distinct layers of SATCLD effective clouds. Thus the mid-tropospheric net radiative cooling rate appears to be very sensitive to cloud type and/or cloud top height. The caveat is that the "convective" SATCLD effective clouds are not radiatively consistent with the satellite-derived fluxes at the top of the atmosphere. Since the system of two equations (equations (1) and (2)) was solved for only one unknown n_t, another free parameter, such as cloud top height, would be needed to enhance the radiative consistency. Note, however, that cloud top height is not infinitely adjustable, since GCM's have finite vertical resolution. Thus one layer of effective cloud with ad-

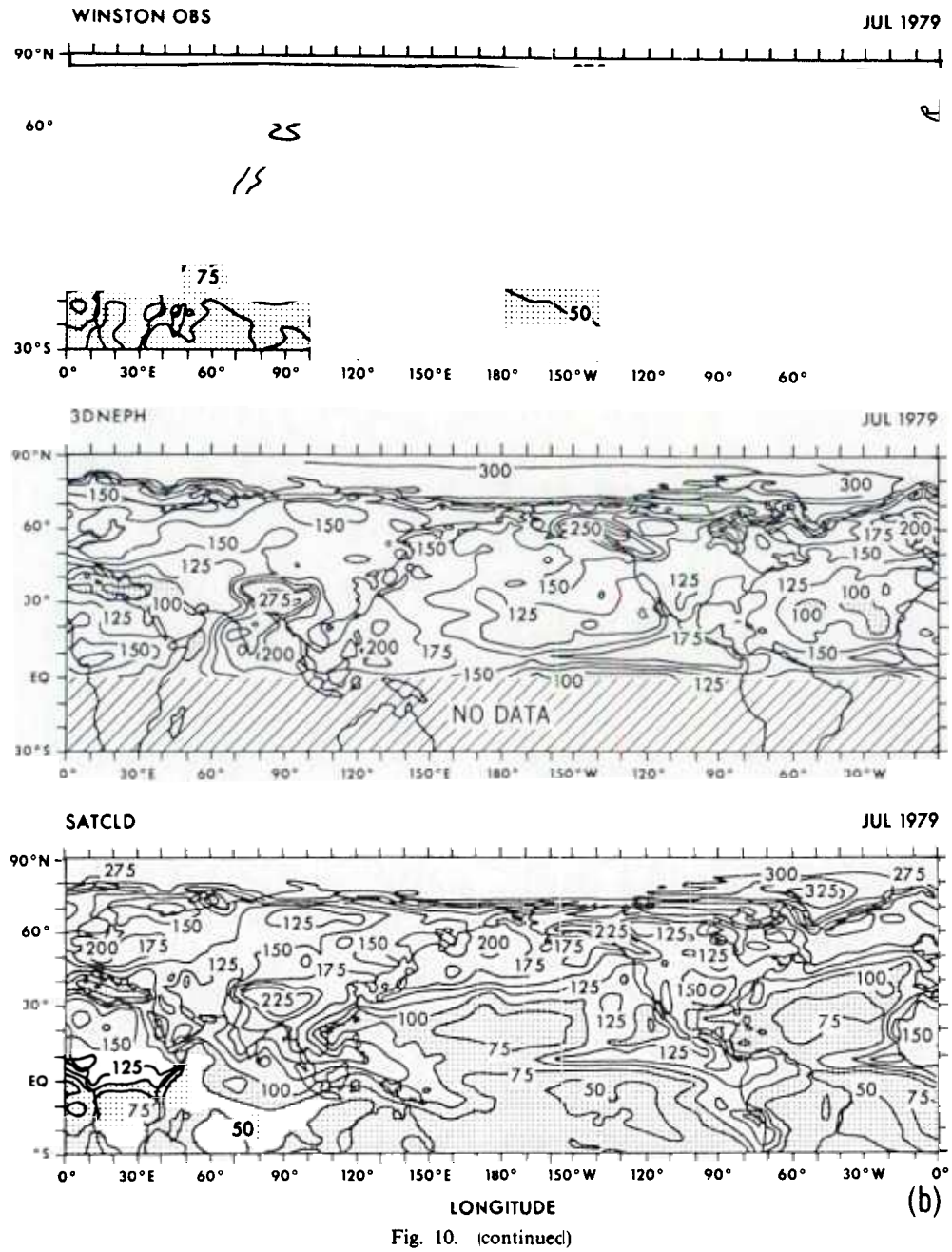

Fig. 10. (continued)

justable cloud top height would generally be less radiatively consistent in GCM's than two distinct layers.

The latitudinal profiles of model-diagnosed net radiative cooling at $\sigma = 0.5$ for July 1979 (Figure 14) reveal a sharp discontinuity near 38°N in the 3DNEPH curve, but not in the SATCLD curve. This discontinuity is related to another in the specified heights of high, and especially middle, clouds in our GCM (see Figure 1*b*) coupled with a moderate amount of 3DNEPH middle cloud ($\langle n_m \rangle \sim 0.17$). It could induce a systematic bias in a GCM's predicted meridional temperature gradient.

Latitude-longitude distributions of SATCLD and 3DNEPH net radiative flux at the earth's surface (not shown) reveal considerable structure in the northern hemisphere in July, when the incoming solar radiation is close to its seasonal maximum there. Overall, both distributions are qualitatively similar. Yet the SATCLD minimum in the North Pacific and SATCLD maxima in the subtropical and eastern tropical oceans are approximately 20 W m^{-2} more intense than their 3DNEPH counterparts. These differences are consistent with differences in SATCLD versus 3DNEPH low cloud amount. The net radiative flux decreases as the low cloud amount increases.

5. Summary of Results

We have formulated a scheme, called SATCLD, for generating fields of effective low and high cloud amount for GCM's from fields of satellite-derived radiative fluxes at the top of the atmosphere. This "poor man's scheme" is economically efficient for two (or three) cloud parameters and requires a minimal amount of data processing, as it utilizes archived analyses of radiative fluxes on a 250-km resolution grid instead of raw radiance data. The results are inherently dependent upon the particular GCM's cloud radiation model, surface albedo field, etc., as well as the "observed" satellite and conventional meteorological data. To demonstrate the application of the

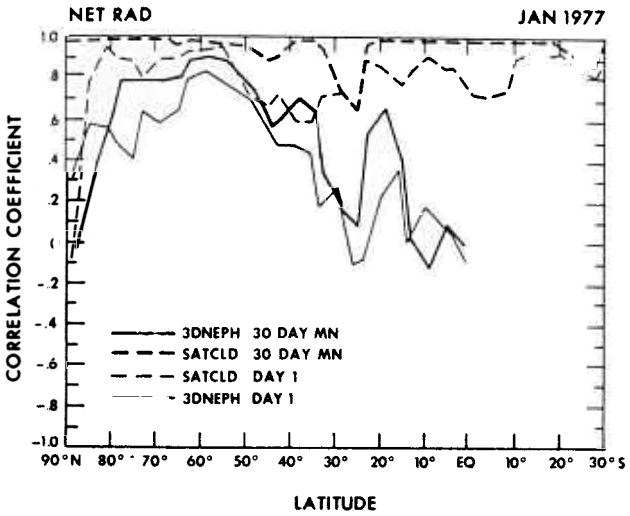

Fig. 11. Longitudinal correlation between model-diagnosed and observed eddy net radiative flux versus latitude for January 1977 monthly mean conditions and January 1, 1977, conditions. Domain is 90°N to 30°S.

scheme, a typical current generation GCM and currently available archived broadband flux data were utilized, despite potentially serious limitations of both. However, the scheme could be applied to future, more accurate observed data sets and improved GCM's.

The underlying approach might be categorized as an inverse method. The analyzed observed shortwave flux S_{obs} and outgoing long-wave flux F_{obs} at each grid point of our GCM were expanded as Taylor series in the unknown effective low and high cloud amounts. The unknowns were determined by trial and error to the nearest 0.01 so as to locally minimize the sum of the squares of the residuals in the Taylor series expansions for S_{obs} and F_{obs}. In this manner the SATCLD analysis of effective low and high cloud amount were also locally constrained to be approximately consistent with the observed net radiative flux at the top of the atmosphere.

Quasi-global SATCLD fields of effective low and high cloud amount were generated by our GCM for two monthly mean cases, i.e., January 1977 and July 1979, as well as some daily mean cases. They were compared with the 3DNEPH and/or SFCOBS analyses of observed cloud amount. In addition, model-diagnosed radiative fluxes were calculated by our GCM, using the above specifications of cloud amount and observed meteorological conditions. Analysis of the above cloud amount fields and corresponding model-diagnosed radiative fluxes helped to reveal qualitative information about GCM- and observation-dependent biases.

In the tropics and subtropics (except over deserts) the radiative budget at the top of the atmosphere was more sensitive to clouds than to surface albedo or surface temperature. In these regions the horizontal distributions of SATCLD low and high effective cloud amount seemed plausible in many respects, based upon comparison with 3DNEPH or SFCOBS. For example, they contained dry zones and well-defined ITCZ's, as did the 3DNEPH. Similarly, in the well-known regions of stratocumulus formation off the west coasts of the Americas and southern Africa, the SATCLD effective low cloud resembled SFCOBS in July. However, there were some substantial differences between analyses in the intensity of the summer ITCZ, "dry zones" over the subtropical east central Pacific Ocean, and convection over the southeastern United States. The effective low cloud amount over the Sahara Desert was presumably unrealistic. Fortunately, it decreased when our standard specification of surface albedo was replaced by CLIMAP's. At mid-latitudes the SATCLD effective low cloud amount field bore some resemblance to the 3DNEPH and/or SFCOBS, mainly over the oceans. In winter the SATCLD effective cloud fields seemed unrealistic over snow-covered mid-latitude terrain, and the scheme appeared to be ill-conditioned in the polar night region. Meanwhile, in summer the SATCLD and 3DNEPH fields of high cloud amount were in quite good agreement. Also, Arctic stratus were better simulated for our improved GCM parameterization of snow albedo than for our standard one.

Several systematic biases in our GCM and in the observed data were linked, mainly by inference, to SATCLD-observed or SATCLD-3DNEPH radiative flux discrepancies or to corresponding unrealistic features of the SATCLD effective cloud amount fields: (1) a diurnal sampling bias in the observed radiative fluxes; (2) a lack of temporal synchronization between satellite and conventional temperature observations; (3) an underestimate of the true surface albedo over the Sahara Desert by our GCM; (4) an inaccurate GCM parameterization of snow albedo; and (5) biases in our GCM's cloud radiation model, e.g., the specification of albedos for middle clouds. The effective high cloud amount was also found to be quite sensitive to the specification of cloud top height.

In July 1979 the discrepancy between DMSP versus TIROS-N measurements of reflected shortwave radiation could have been large. But in January 1977, when the AFGWC utilized NOAA 5 satellite data, other factors must have been predominantly responsible for the SATCLD-3D-Neph discrepancies. Some possibilities include inadequate GCM specifications of surface and cloud albedos, especially for middle level clouds; insufficient information in the AFGWC 3DNEPH to deduce the true thickness and hence albedo of middle clouds or of low- to middle-level cloud systems; and a positive bias in the 3DNEPH total cloud cover in relatively cloudy regions, e.g., the ITCZ. But overall, neither the January 1977 nor July 1979 SATCLD-3DNEPH discrepancies have been definitively explained.

In conclusion we believe that currently available, and in the foreseeable future, new cloud amount data sets would not necessarily yield GCM-diagnosed radiative fluxes that were

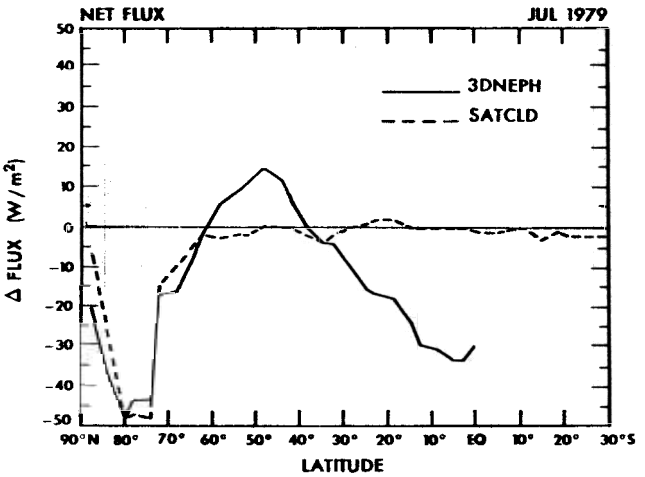

Fig. 12. Differential (i.e., model-diagnosed minus observed) zonal monthly mean net radiative fluxes for July 1979. Domain is 90°N to 30°S.

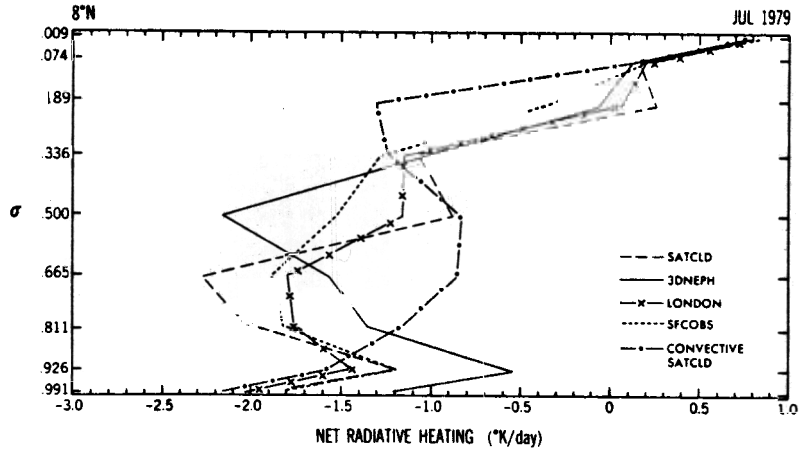

Fig. 13. Vertical profiles of zonal monthly mean net radiative heating rate (K d^{-1}) for July 1979 and various specifications of cloud amount. The latitude is 8°N.

consistent with satellite observations for every GCM. Therefore, GCM-dependent, radiatively adjusted—i.e., initialized—clouds might be a useful alternative, in the interim, for some prognostic applications of GCM's. In this light the SATCLD methodology could be viewed as a feasible, economical approach by which modelers could generate their own analyses of (effective) cloud amount and hence quasi-realistic cloud-radiation forcing for their GCM's.

At the same time it is desirable that discrepancies between effective versus real clouds be reduced without incurring a substantial loss in radiative consistency. To achieve this goal, currently available GCM cloud radiation models and treatment of surface albedo as well as archived satellite data must be improved. Similarly, the SATCLD algorithm should be generalized to incorporate more parameters that characterize real clouds, and the results should be independently verified. In any case, producers of observed or climatological cloud amount data sets should be encouraged to archive observed radiative fluxes and assumed surface albedos, along with the actual cloud data, at a horizontal resolution characteristic of GCM's.

As another means of reducing discrepancies between effective versus real clouds, auxiliary cloud parameters, such as cloud top heights and emissivities, could be obtained directly from future ISCCP cloud data sets. SATCLD would then function more explicitly as a cloud radiation initialization scheme for GCM's.

6. Some Suggestions for Improving the SATCLD Analyses

The treatment of surface albedo in our GCM has already been substantially improved by replacing the *Posey and Clapp* [1964] specification with the CLIMAP specification and by incorporating the effects of snowmelt (as well as underlying vegetation) into our GCM parameterization of snow albedo. The results seem to be encouraging. But visible and near-infrared spectral reflectivities of snow and vegetative cover still need to be incorporated. Perhaps satellite-measured spectral

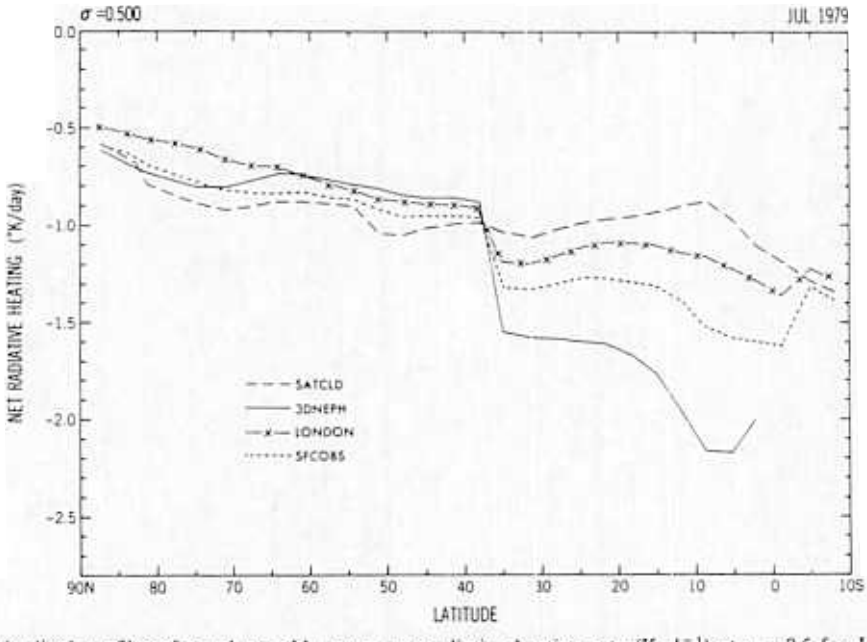

Fig. 14. Latitudinal profiles of zonal monthly mean net radiative heating rate (K d^{-1}) at $\sigma = 0.5$ for July 1979 and various specifications of cloud amount. The domain is 90°N to 10°S.

reflectances in the visible and near infrared and/or 10-day or monthly mean minimum brightness information could be utilized.

Any means of improving the model-diagnosed vertical profile of net radiative cooling would be desirable, since the latter is probably even more important for the atmospheric circulation than the radiative budget at the top of the atmosphere is [*Stephens and Webster*, 1981; *Shukla and Sud*, 1981], especially on a time scale of 0(1 month) or less. The present specification of cloud tops must introduce some bias. However, the height of high cloud tops could perhaps be specified as a function of longitude as well as latitude, with the aid of vertical temperature sounding data or future ISCCP cloud data. But to properly utilize such information, the vertical resolution of our nine-level GCM would have to be refined in the upper troposphere.

In principle the SATCLD scheme could be generalized to incorporate more cloud parameters that characterize real clouds, such as effective liquid/ice water content (or equivalently, reflectivity and emissivity) or effective middle-cloud amount. An abortive attempt was made to treat middle-level clouds by introducing a third unknown n_m and corresponding derivative terms into equations (1) and (2) as well as a physical realizability constraint for n_m analogous to equations (4*a*) and (4*b*). But unfortunately, the partitioning between SATCLD low versus middle effective cloud amounts contained considerable computational noise. It is conjectured that the system of two equations and only one minimization constraint for three unknowns was underdetermined. An additional equation and minimization constraint could be incorporated if an archive of quasi-independent observed radiative flux data becomes available. *Diak et al.* [1982] have demonstrated the feasibility of determining the surface insolation from geostationary satellite data. In situ measurements of radiative fluxes in the midtroposphere or satellite-derived measurements from additional spectral bands, (e.g., 1.6 μm or 3.6 μm) are two other possibilities.

The availability of more than two parameters could be used to independently verify effective cloud fields and, hence, GCM cloud radiation models. F. Bretherton's idea, proposed in *FIRE* [1983] is to work with an overdetermined system of equations. Some spectral radiance data would be used to determine various cloud properties. Meanwhile, radiance data from other channels would be used to independently verify a GCM's cloud radiation model against a state of the art, one-dimensional column model.

To help control the temporal synchronization problem in July 1979 (as well as incorporate improved meteorological analyses for the tropics), diurnal mean or local time (asynoptic) fields of model-diagnosed long-wave flux could be estimated from the 2-hourly archive of the GFDL FGGE four-dimensional analysis of meteorological data. Also, monthly mean model-diagnosed radiative fluxes could be averaged from twice-daily diagnosed fluxes in order to represent potentially significant nonlinear radiative effects associated with transient synoptic disturbances.

Modelers should also perform controlled sensitivity experiments to become more aware of characteristics (including biases) of different satellite observational systems and modeling assumptions used to retrieve the data, as well as their impact on effective clouds. For example, TIROS-N, Nimbus 7, and GOES earth radiation budget data offer considerable diversity with regard to sampling times, sampling frequency, spectral bandwidth, and/or assumptions about bidirectional reflectance. Some preliminary results of a TIROS-N versus Nimbus 7 intercomparison have been reported recently by *Gordon* [1984].

Finally, the sensitivity of the long-range predicted atmospheric circulation to quasi-realistic cloud radiation forcing, as imposed through SATCLD effective clouds, is currently being examined. These experiments will be the subject of a future paper.

Acknowledgments. The authors wish to thank S. B. Fels, R. T. Wetherald, and M. D. Schwarzkopf for reviewing the manuscript and offering many valuable suggestions. The manuscript was typed by Betty Williams and Joan Pege. The figures were drafted by P. Tunison and W. Ellis and photographed by J. Conner.

REFERENCES

Bignell, K. J., The water-vapor infra-red continuum, *Q. J. R. Meteorol. Soc.*, *96*, 390–403, 1970.

Cess, R. D., B. P. Briegleb, and M. S. Lian, Low-latitude cloud amount and climate feedback: Comparative estimates from satellite data, *J. Atmos. Sci.*, *39*, 53–59, 1982.

Diak, G. R., C. Gautier, and S. Masse, An operational system for mapping insolation from GOES satellite data, *Solar Energy*, *28*, 371–376, 1982.

Fels, S. B., and M. D. Schwarzkopf, The simplified exchange approximation: A new method for radiative transfer calculations, *J. Atmos. Sci.*, *32*, 1476–1488, 1975.

Fels, S. B., and M. D. Schwarzkopf, An efficient, accurate algorithm for calculating CO_2 15-μm band cooling rates, *J. Geophys. Res.*, *85*(C2), 1205–1232, 1981.

First ISCCP Regional Experiment (FIRE), The research plan for FIRE, A U.S. program in the context of the International Satellite Cloud Climatology Project (ISCCP), report, U.S. Nat. Clim. Program Office, Washington, D.C., 1983.

Fye, F. K., The AFGWC automated cloud analysis model, *Tech. Memo. 78-002*, 97 pp., Air Force Global Weather Central, Offut Air Force Base, Nebr., 1978.

Gordon, C. T., The specification of radiatively constrained, effective clouds in GCM's: Methodology and some preliminary results, paper presented at Workshop on Cloud Cover Parameterization Schemes in Large-Scale Numerical Models: Design, Validation, and Dynamical Impact, Eur. Centre for Medium-Range Weather Forecasts, Reading, England, November 26–28, 1984.

Gordon, C. T., and W. F. Stern, A description of the GFDL global spectral model, *Mon. Weather Rev.*, *110*, 625–644, 1982.

Gordon, C. T., R. Hovanec, and W. F. Stern, Analyses of monthly mean cloudiness and their effect on GCM-diagnosed radiative fluxes, *J. Geophys. Res.*, *89*(D3), 4713–4738, 1984.

Gruber, A., Determination of the earth-atmosphere radiation budget from NOAA satellite data, *NOAA Tech. Rep. NESS 76*, Nat. Environ. Sat. Serv., Washington, D. C., 1978.

Lacis, A. A., and J. E. Hansen, A parameterization for the absorption of solar radiation in the earth's atmosphere, *J. Atmos. Sci.*, *31*, 118–132, 1974.

Mellor, G. L., and T. Yamada, A hierarchy of turbulence closure models for planetary boundary layers, *J. Atmos. Sci.*, *31*, 1791–1806, 1974.

Meleshko, V. P., and R. T. Wetherald, The effect of a geographical cloud distribution on climate: A numerical experiment with an atmosphere general circulation model, *J. Geophys. Res.*, *86*(C12), 11,995–12,014, 1981.

Minnis, P., and E. F. Harrison, Diurnal variability of regional cloud and clear-sky radiative parameters derived from GOES data, 2, November 1978 cloud distributions, *J. Clim. Appl. Meteorol.*, *23*, 1012–1031, 1984.

Ohring, G., A Gruber, and R. G. Ellingson, Satellite determination of the relationship between total longwave radiation flux and infrared window radiance, *J. Clim. Appl. Meteorol.*, *23*, 416–425, 1984.

Payne, R. E., Albedo of the sea surface, *J. Atmos. Sci.*, *29*, 959–970, 1972.

Ploshay, J. J., R. K. White, and K. Miyakoda, FGGE level III-B daily global analyses, 1, *NOAA Data Rep. ERL GFDL-1*, Geophys. Fluid Dyn. Lab., Princeton, N. J., 1983.

Posey, M. W., and P. F. Clapp, Global distributions of normal surface albedo, *Geofis. Int.*, *4*(1), 33–48, 1964.

Ramanathan, V. E., E. J. Pitcher, R. C. Malone, and M. L. Blackmon,

The response of a spectral general circulation model to refinements in radiative processes, *J. Atmos. Sci.*, *40*, 605–630, 1983.

Robinson, D. A., Anthropogenic impact on winter surface albedo, Ph.D. thesis, Lamont-Doherty Geol. Observ., Columbia Univ., Palisades, N. Y., 1984.

Robock, A., The seasonal cycle of snow cover, sea ice and surface albedo, *Mon. Weather Rev.*, *108*, 267–285, 1980.

Sasamori, T., J. London, and D. V. Hoyt, Radiation budget of southern hemisphere, *Meteorol. Monogr.*, *13*, 9–23, 1972.

Schneider, S. H., Cloudiness as a global climatic feedback mechanism: The effects on the radiation balance and surface temperature of variations in cloudiness, *J. Atmos. Sci.*, *29*, 1413–1422, 1972.

Shukla, J., and Y. Sud, Effect of cloud-radiation feedback on the climate of a general circulation model, *J. Atmos. Sci.*, *38*, 2337–2353, 1981.

Slingo, J. M., Cloud cover experimentation with the ECMWF model, paper presented at Workshop on Cloud Cover Parameterization Schemes in Large Scale Numerical Models: Design, Validation, and Dynamical Impact, Eur. Centre for Medium-Range Weather Forecasts, Reading, England, November 26–28, 1984.

Stephens, G. L., and P. J. Webster, Sensitivity of radiative forcing to variable cloud and moisture, *J. Atmos. Sci.*, *36*, 1542–1556, 1979.

Stephens, G. L., and P. J. Webster, Clouds and climate: Sensitivity of simple systems, *J. Atmos. Sci.*, *38*, 235–247, 1981.

Stowe, L. L., P. P. Pelligino, and P. H. Hwang, Validation of Nimbus 7 cloud products, paper presented at IAMAP International Radiation Symposium, Perugia, Italy, August 21–29, 1984.

Taylor, V. R., and L. L. Stowe, Reflectance characteristics of uniform earth and cloud surfaces, *J. Geophys. Res.*, *89*(D4), 4987–4996, 1984.

Telegadas, K., and J. London, A physical model of the northern hemisphere troposphere for winter and summer, *Sci. Rep. 1, Contract AF 19(122)-165, DOC AD 032472*, 55 pp., Res. Div., Coll. Eng., N. Y. Univ., New York, 1954.

Warren, S. G., and W. J. Wiscombe, A model for the spectral albedo of snow, 2, Snow containing atmospheric aerosols, *J. Atmos. Sci.*, *37*, 2734–2745, 1980.

Wiscombe, W. J., and S. G. Warren, A model for the spectral albedo of snow, 1, Pure snow, *J. Atmos. Sci.*, *37*, 2712–2733, 1980.

C. T. Gordon and W. F. Stern, Geophysical Fluid Dynamics Laboratory, Princeton University, P.O. Box 308, Princeton, NJ 08542.

R. D. Hovanec, Kidder, Peabody and Company, Inc., 120 Broadway, New York, NY 10271.

(Received March 26, 1984;
revised June 7, 1985;
accepted June 7, 1985.)